JOURNAL OF GEOPHYSICAL RESEARCH, VOL. 104, NO. D8, PAGES 9337–9359, APRIL 27, 1999

A one and half year interactive MA/ECHAM4 simulation of Mount Pinatubo Aerosol

Claudia Timmreck, Hans-F. Graf, and Ingo Kirchner

Max–Planck–Institut für Meterologie, Hamburg, Germany

Abstract. The Mount Pinatubo volcanic eruption in June 1991 had significant impact on stratospheric and tropospheric climate and circulation. Enhanced radiative heating caused by the aerosol absorption of solar and terrestrial radiation changed stratospheric temperature and circulation. Using the stratospheric mesospheric version of the Hamburg climate model MA/ECHAM4, we performed an interactive Pinatubo simulation with prognostic stratospheric aerosol. Interactive and noninteractive model results for the years 1991 and 1992 are compared with satellite data and in situ measurements. The on–line calculated heating rates are in good agreement with radiation transfer models indicating maximum heating rates of about 0.3 K/d in October 1991. The dynamic feedback in the MA/ECHAM4 simulation is similar to observations. The model is able to reproduce the strengthening of the polar vortex in winter 1991/1992 and a minor warming in January. The importance of an interactive treatment of the volcanic cloud for the aerosol transport is evidenced by the analysis of effects such as aerosol lifting and meridional transport. In general, the model results agree well with observations from the northern midlatitudes, especially in the first months after the eruption. The MA/ECHAM4 model is successful in reproducing the formation of two distinct maxima in the optical depth but is unable to simulate the persistence of the tropical aerosol reservoir from the end of 1991. Better agreement may be achieved if the influence of the quasi–biennial oscillation and ozone changes is also taken into account.

1. Introduction

The Mount Pinatubo volcanic eruption (15.14°N, 120.35°E) on June 15–16, 1991, had significant impact on stratospheric and tropospheric climate and circulation. During the eruption, 14–26 Mt SO_2 [*Krueger et al.*, 1995] were released into the stratosphere and quickly converted to H_2SO_4 with an e–folding time of 35 days [*Bluth et al.*, 1992; *Read et al.*, 1993]. The eruption took place during the easterly phase of the quasi–biennial oscillation (QBO). The volcanic cloud rapidly moved westward and encircled the Earth within 22 days. In the first months after the eruption the bulk of the aerosol mass was bound in a latitude band between 20°S and 30°N [*McCormick and Veiga*, 1992; *Stowe et al.*, 1992]. Transport of Mount Pinatubo aerosol to the northern middle and high latitudes was mainly connected to synoptic scale processes in the lower stratosphere and the transition from summer to winter circulation in the middle and upper stratosphere [*Trepte et al.*, 1993]. One year after the eruption the volcanic aerosol was globally distributed in latitude band structures with minima in the subtropical region [*Trepte et al.*, 1994]. In spring 1992 the stratospheric aerosol burden had reached its maximum and started to descend and to decrease. Four to five years after the eruption the background level was reached again.

The increased aerosol concentration after the eruption changed the radiative balance of the atmosphere. In summer and autumn 1991 a reduction in the net flux of about 3 to 10 W/m^2 at the top of the atmosphere (TOA) was detected [*Minnis et al.*, 1993; *Dutton and Christy*, 1992]. Also observed were a temperature increase in the lower stratosphere of about 2–3 K [*Labitzke and McCormick*, 1992; *Labitzke*, 1994], a cooling of the global lower troposphere and the Earth surface of about 0.5 K [*Dutton and Christy*, 1992], and a winter warming of the Northern Hemisphere continents [*Robock and Mao*, 1992]. The observed pole-to-equator temperature gradient led to an enhanced polar vortex and a wave response in the tropospheric circulation [*Graf et al.*, 1993; *Kodera*, 1994; *Robock and Mao*, 1995]. The chemical composition of the atmosphere (mainly ozone and ozone relevant chemical species) was also significantly affected after the volcanic eruption [*Grant et al.*, 1992; *Johnston et al.*, 1992; *Coffey and Mankin*, 1993; *Hofmann and Oltmanns*, 1993; *Koike et al.*, 1994; *Coffey*, 1996]. In

Paper number 1999JD900088.
0148-0227/99/1999JD900088$09.00

1992 and 1993 an extraordinary strong ozone reduction due to chemical and dynamical processes was detected [*Grant et al.*, 1994; *Herman and Larko*, 1994; *Randel et al.*, 1995]. Ozone losses could have been caused by heterogeneous reactions at the surface of the sulfuric acid particles, which led to an increase in active chlorine species and therefore to increased ozone destruction [*Hofmann and Solomon*, 1989; *Brasseur and Granier*, 1992; *Prather*, 1992; *Solomon et al.*, 1996]. Ozone changes could also be caused by circulation changes due to the enhanced radiative heating after such a large eruption [*Kinne et al.*, 1992; *Schoeberl et al.*, 1993].

The Pinatubo episode with its large amount of observations provides a unique opportunity to study the climate impact of volcanic eruptions and investigate the role of heterogeneous reactions in the depletion of stratospheric ozone. Several simulations were carried out to study these effects of the Pinatubo eruption, which cover a wide range of subjects. Some of them focus on the climate impact of the volcanic aerosol [*Hansen et al.*, 1992; *Graf et al.*, 1993; *Pitari*, 1993; *Hansen et al.*, 1996; *Graf et al.*, 1996; *Stenchikov et al.*, 1998; *Kirchner et al.*, 1998] and others on the microphysical and chemical effects in the atmosphere after the eruption [*Tie et al.*, 1994; *Kinnison et al.*, 1994; *Bekki and Pyle*, 1994; *Zhao et al.*, 1995; *Weisenstein et al.*, 1997].

The influence of a volcanic disturbance on atmospheric chemistry and dynamics can only be studied if all processes are taken into account and simulated properly. One essential element is the global dispersal of the aerosol cloud. General circulation models (GCMs) with prognostic aerosols are therefore a suitable tool for a complete study of the atmospheric changes caused by the Mount Pinatubo eruption. Up to now there have been only a few GCM simulations published of Mount Pinatubo aerosol with advected volcanic aerosol [*Boville et al.*, 1991; *Pudykiewicz et al.*, 1995]. They consider periods no longer than half a year and neglect the radiative effects of the Pinatubo eruption. However, three-dimensional (3-D) Pinatubo transport simulations showed that the dynamic response to local aerosol heating has an important influence on the initial dispersal of the volcanic cloud. In their Pinatubo simulation with an off-line transport model, *Young et al.* [1994] pointed out that local aerosol heating combined with aerosol lifting to higher altitudes could be the main reason for the observed cross-equatorial transport of the volcanic cloud between days 6 and 12 after the eruption. Using the mechanistic United Kingdom's Meteorological Office (UKMO) stratosphere–mesosphere model (SMM), *Fairlie* [1995] also demonstrated that the equatorial displacement of the cloud was found to be quite sensitive to the definition of the heating profile. In order to properly simulate the impact of aerosol-induced radiative heating on the tracer transport, a fully coupled general circulation model is necessary, where not only the transport of the Pinatubo cloud but also the volcanic-induced heating are calculated on-line. In addition, Pinatubo studies with the ECHAM4 climate model and prescribed aerosol by *Stenchikov et al.* [1998] and *Kirchner et al.* [1998] have already demonstrated that the climate model is able to reproduce the observed globally averaged cooling signal. In previous noninteractive Pinatubo simulations using three different vertical versions of the ECHAM4 climate model (ECHAM4 L19, ECHAM4 L39, MA/ECHAM4), *Timmreck et al.* [1999] have shown that the on-line calculated heating rates agree well with published data. These simulations were in good agreement with satellite data for the first months after the eruption. All model versions were, however, unable to simulate the initial cross-equatorial transport. Some months after the eruption, differences occurred in the global dispersion of the cloud between the simulations and observations.

Here we will present results of an interactive Pinatubo simulation with the Middle Atmosphere ECHAM (MA/-ECHAM4) [*Manzini et al.*, 1997]. The global transport of the volcanic cloud and the aerosol-induced heating will be calculated on-line. The focus of this study is the influence of an interactive treatment on the global transport of the volcanic cloud. In comparing interactive and noninteractive MA/ECHAM4 simulations with various observations, we will point out differences in the transport pattern and discuss further possible influences.

2. Model Description

For our experiments we used the stratospheric mesospheric version of the Hamburg climate model ECHAM4 [*Roeckner et al.*, 1996], the MA/ECHAM4 [*Manzini et al.*, 1997], which is based on primitive equations. The prognostic variables are vorticity, divergence, (logarithm of) surface pressure, temperature, water vapor, and cloud (liquid and ice) water content. The MA/ECHAM4 extends from the surface to 0.01 hPa and is divided into 39 hybrid sigma pressure levels. Near the tropopause the vertical resolution is about 1.5 km and slowly decreases with height to about 2 km at 50 hPa, 3 km at 30 hPa, and 7 km at the model top. Doppler spread parameterization and gravity wave momentum deposition are also included in the model. For a detailed model description of the MA/ECHAM4, see *Manzini et al.* [1997].

The MA/ECHAM is run with a spectral triangular truncation at wavenumber 30 (T30) resolution. Physical processes and nonlinear terms are calculated on a Gaussian longitude–latitude grid with a nominal resolution of 3.75° × 3.75°. In the model, a semi-Lagrangian transport scheme [*Williamson and Rasch*, 1989] is applied for the tracer transport. A semi-implicit leapfrog time integration is used with a time step of 30 min for both the dynamics and the physics, while the radiation scheme is calculated only every 2 hours.

The MA/ECHAM4 radiation scheme is based on a

two-stream method with eight spectral intervals, two in the solar [*Fouquart and Bonnel,* 1980] and six in the terrestrial [*Morcrette,* 1991]. The radiation scheme also considers absorption of greenhouse gases (H_2O, CO_2, O_3, CH_4, N_2O, and 16 CFCs) (R. van Dorland, personal communication, 1995) as well as scattering and absorption by clouds and aerosols. Furthermore, the radiation model can take into account prognostically calculated aerosol types. Optical parameters of the aerosols types are calculated from the time dependent aerosol mass mixing ratio, normalized extinction and absorption coefficients, and a normalized asymmetry factor.

In a previous Pinatubo simulation with the ECHAM4 L19 [*Timmreck et al.,* 1999] the global transport of the volcanic cloud turned out to be the most critical point. A detailed microphysical description of the volcanic aerosol is not only expensive but also useful only if the global transport is well represented in the model. Thus this set of simulations does not explicitly consider detailed microphysical processes such as nucleation, coagulation, condensation, and sedimentation. The H_2O/H_2SO_4 aerosol is considered with a bulk approach and described by the mass mixing ratio of sulfate (SO_4^{2-}). For the radiative calculation we assume a typical background distribution [*Pinnick et al.,* 1976] with a mode radius r_m of 0.075 μm and a standard deviation σ_s of 1.8 as a first approximation. Observations after the Pinatubo eruption show that the volcanic size distribution was highly variable in time and space [*Russell et al.,* 1996]. Thus a "typical volcanic" distribution would also be only an approximation, which is better suited for the observed aerosol distribution in some areas of the globe but not to all. The only adequate consideration of the volcanic size distribution in a model with prognostic volcanic aerosol is the on-line calculation of microphysical processes, which is, at present, not favorable.

In order to investigate the uncertainties in the MA/-ECHAM4 radiation calculation due to different size distribution, *Timmreck et al.* [1999] performed sensitivity tests for four different size distributions with the 1-D version of the ECHAM4 radiation code and a constant tropical aerosol profile in August 1991. The heating rate profiles were clearly dominated by the mass mixing ratio, with highest values for the maximum concentration. Differences in the on-line calculated radiative heating rates between different aerosol size distributions were of the order of about 15%. However, these deviations were small in comparison to those that would be caused by changes in the aerosol concentration due to incorrect transportation. Therefore it is, first of all, important to properly simulate the observed transport pattern combined with a correct representation of the aerosol mass profile. Then, in a second step the temporal development of the aerosol size distribution has to be taken into account. Nevertheless, the importance of the consideration of detailed microphysical processes for the radiative calculation should be emphasized. Overall, we think that for our purpose the selected size distribution is appropriate, but it is certainly not sufficient for a realistic determination of climate forcing.

For the current study a sulfur cycle [*Feichter et al.,* 1996] is coupled to the meteorological model, which takes into account the oxidation pathways of sulfur dioxide SO_2 and the removal processes of SO_2 and SO_4^{2-} in the troposphere. The sulfur cycle calculates transport, emission, chemistry, and wet and dry deposition of dimethylsulfide (DMS), SO_2, and SO_4^{2-}. Anthropogenic and volcanic emissions are released as SO_2 and biogenic emissions as DMS. In the gas phase, SO_2 and DMS react with OH, whereby the only end product of DMS oxidation is assumed to be SO_2. SO_2 is dissolved in cloud water and oxidized by both hydrogenperoxide (H_2O_2) and ozone (O_3). For the chemical conversion rates, monthly mean oxidant concentrations are prescribed from ECHAM calculations [*Roelofs and Lelieveld,* 1995; *Steil et al.,* 1998] and from a 2-D simulation [*Grooß et al.,* 1998]. The dry deposition is considered different for land, sea, and snow, and the rain-out of the dissolved sulfur species is calculated in terms of the model's precipitation formation rate. For a detailed description of the model, see *Feichter et al.* [1996]. In the stratosphere, SO_2 is directly converted with OH into sulfate, which means that the conversion rate may become increasingly overestimated with time.

Previous Pinatubo simulations with the ECHAM4 L19 (top 10 hPa) and the MA/ECHAM4 (top 0.01 hPa) show an overestimated decay of the volcanic aerosol mass [*Timmreck et al.,* 1999]. Owing to numerical diffusion, the simulated volcanic aerosol was rapidly transported downward into the troposphere, where it was removed within several days by wet and dry deposition. In order to reduce the model bias of an overstrong advective vertical transport across the tropopause, an artificial damping has been introduced in the model [*Timmreck et al.,* 1999], which improves the model results, especially in the first months after the eruption. The damping is based on the reduction of the advective vertical transport in the 380 K layer by 75%. In order to avoid steep gradients, the vertical transport is also reduced by 25% in the layer above and below the 380 K layer. Owing to this assumption, the seasonal variability of the stratosphere-troposphere exchange (STE) is not disturbed; only the strength of the exchange is reduced, while the total mass is unchanged.

In the following, two Pinatubo experiments are investigated: an interactive simulation, where the volcanic aerosol is taken into account by the radiation scheme of the model, and a noninteractive one, where the aerosol has no influence on the radiation. In analogy to the ECHAM4 L19 Pinatubo simulation [*Timmreck et al.,* 1999] we assume an initial volcanic cloud mass of 17 Mt SO_2, according to Microwave Limb Sounder (MLS) and total ozone mapping spectrometer (TOMS)

observations [*Read et al.*, 1993; *Krueger et al.*, 1995]. In the horizontal the Pinatubo cloud is initialized over 19 grid boxes between 0° – 18.55°N and 96°E – 118°E, corresponding with TOMS observations of June 16, 1991 [*Bluth et al.*, 1992]. In the vertical the initial SO_2 mass is distributed over four model layers between 61 and 21 hPa (19 and 27 km). This corresponds to lidar observations, which have shown that the volcanic plume reached up to a height of 30 km, with the bulk of the aerosol between 20 and 27 km [*McCormick et al.*, 1995]. In order to obtain meteorological conditions comparable with observations during this time, daily observed sea surface temperatures (SSTs) are prescribed based on European Centre for Medium-Range Weather Forecasts (ECMWF) data.

3. Results

3.1. Calculation of Radiative Properties

In order to obtain information about additional aerosol–induced radiative heating, the radiation code in the MA/ECHAM4 simulation is called twice with and without the consideration of sulfate aerosol. Radiative calculations were also performed for clear–sky conditions. Radiative heating and net radiative fluxes in our model are estimated from the difference between the radiation calculations in the interactive MA/ECHAM4 simulation (interactive simulation with aerosol minus interactive simulation without aerosol). Thus we do not determine the radiative forcing in our simulation, we only estimate the additional aerosol heating due to the volcanic aerosol.

Figure 1 shows the zonal mean vertical profiles of radiative heating in both the solar (0.25–4 μm) and the terrestrial (4–250 μm) bands of the ECHAM radiation scheme and the sum of both for August and October 1991. In both months the effect of the Intertropical Convergence Zone (ITCZ) is clearly shown in the double structure of the simulated heating rates with prognostic aerosol. A distinct tropical minimum in the heating rates is found at 10°N in August and at 3°N in October. Aerosol-induced heating with values larger than 0.01 K/d is located between 50°S and 50°N. In August, additional enhanced radiative heating of 0.01 K/d occurs in a small band between 40 hPa and 100 hPa north of 30°N. This feature corresponds well with lidar measurements, which detected Pinatubo aerosol in July in northern midlatitudes [*Jäger*, 1992]. In contrast to August, the solar irradiance in October is not strong enough to produce a volcanically induced heating over 0.01 K/d in high northern latitudes. Aerosol lifting through aerosol–induced heating is clearly indicated in the increase of the maximum height of the simulated 0.2 K/d cloud in the MA/ECHAM simulation between August and October in the Northern Hemisphere.

A separation of the volcanically induced heating rates in the spectral intervals of the ECHAM radiation scheme shows distinct differences between the terrestrial and the solar bands. In the terrestrial part of the spectrum the maximum heating rate of 0.1 K is found between 15 and 50 hPa owing to enhanced absorption of longwave radiation in the aerosol–containing layers. Above this region, reduced heating is calculated by the model because less terrestrial radiation reaches this altitude and the aerosol irradiates more into space. These cooling is more distinctive in October than August. In the tropical troposphere, minor heating is caused by ozone and water vapor absorption of enhanced downward longwave radiation. In the solar part of the spectrum the heating maximum is located at higher altitudes between 5 and 15 hPa in August and between 3 and 13 hPa in October. A slight cooling due to less absorption by water vapor is also found in the troposphere.

In October the total heating, with maximum rates of 0.3 K/d, corresponds well with *Kinne et al.* [1992], while the contribution of the solar part of the total heating does not. A possible explanation for this difference might be the selected aerosol distribution. Owing to the assumption of a background distribution, more but smaller particles are considered compared to a volcanic size distribution. Thus solar heating is overestimated and terrestrial is underestimated. An additional reason might also lie in the broad range of the two solar bands of the ECHAM4 radiation scheme (0.25–4 μm), which encompasses not only the visible part of the spectrum but also the near infrared (IR). In a ECHAM4 L19 experiment with prescribed Pinatubo aerosol by *Stenchikov et al.* [1998], the visible and the near–IR spectral bands of the ECHAM4 radiation scheme were regarded separately. This more detailed comparison of the Pinatubo–induced heating showed that the maximum heating in the near–IR is as strong as the maximum heating in the IR.

Overall, the simulated total heating rates are in good agreement with both the results of ECHAM4 L19 simulations by *Stenchikov et al.* [1998] using the Pinatubo aerosol data set (PADS) and other literature data [*Kinne et al.*, 1992; *Tie et al.*, 1994; *Fairlie*, 1995]. In the following sections we will investigate the way in which the global transport is influenced by this additional heating.

3.2. Influence of Stratospheric Transport

Figure 2 shows the initial dispersal of the total SO_2 column amount (matm cm) 4, 8, 12, and 14 days after the eruption for the noninteractive MA/ECHAM4 simulation, and Figure 3 shows the respective dispersal for the interactive simulation. The SO_2 cloud moves rapidly westward in both simulations corresponding well with TOMS observations [*Bluth et al.*, 1992]. After 4 days both simulations, are in good agreement with the bulk of the Pinatubo cloud located between east Africa and India. Eight days after the eruption, differences between the noninteractive and the interactive simulation begin to develop. The volcanic cloud in the inter-

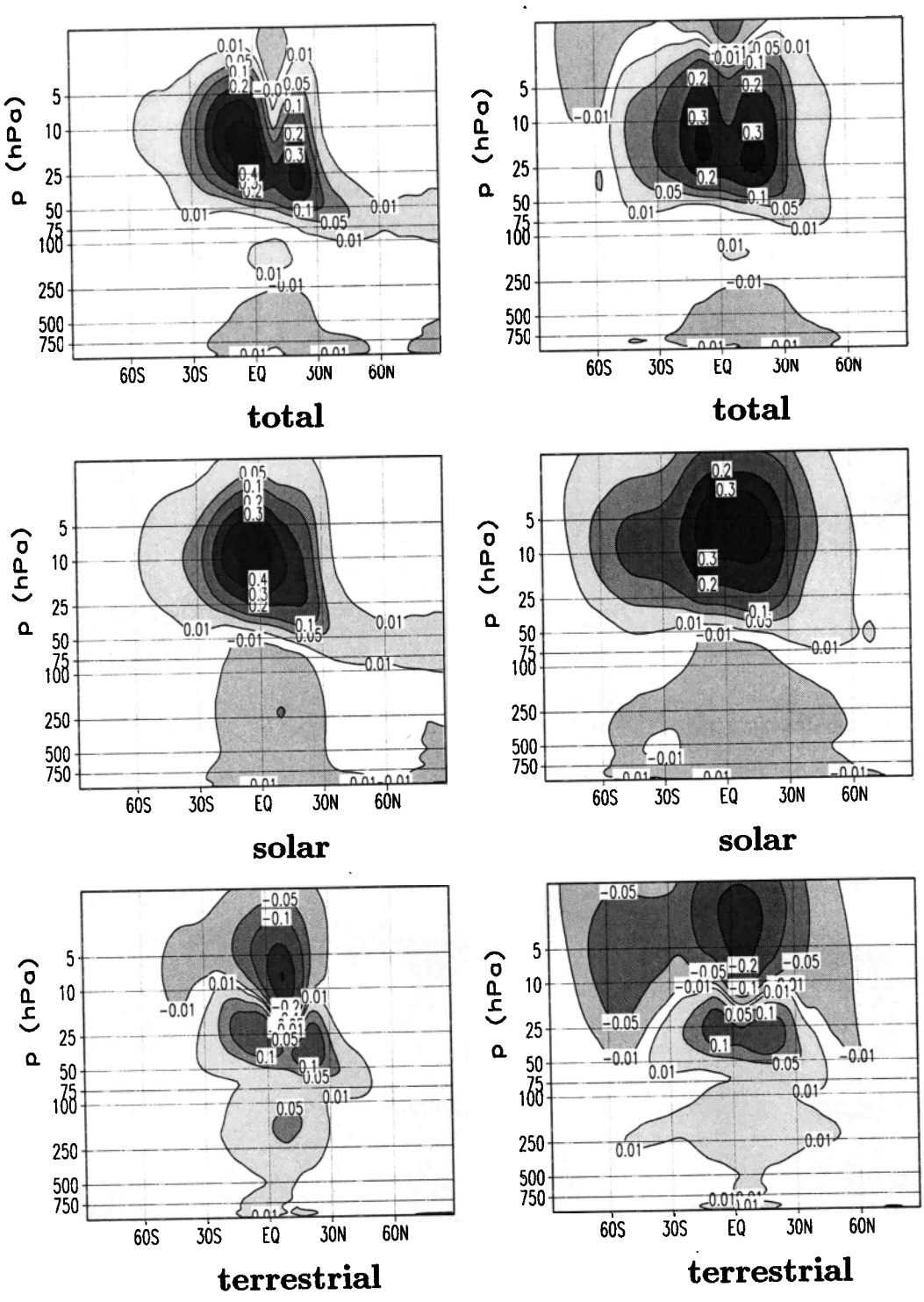

Figure 1. Simulated perturbation of the zonal and monthly mean heating rates (K/d) in the interactive MA/ECHAM4 model run caused by the Pinatubo eruption for (left) August 1991 and (right) October 1991 for the (top) total, (middle) solar (0.25-4 μm), and (bottom) terrestrial (4-250 μm) spectral bands.

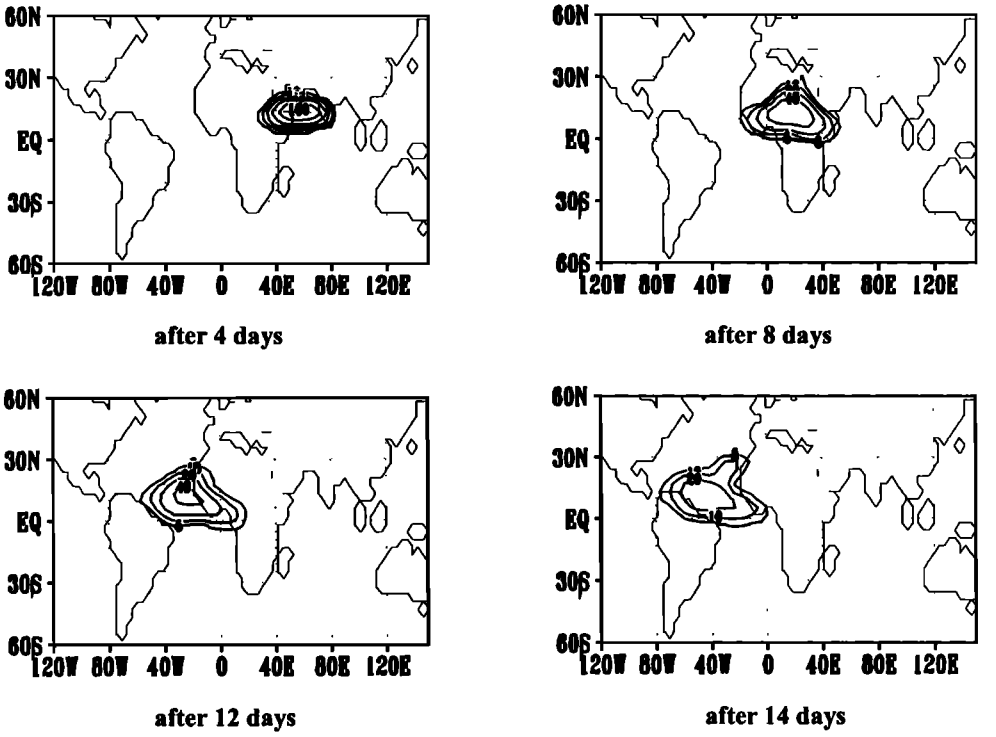

Figure 2. Initial dispersal of the SO_2 column amount (matm cm) 4, 8, 12, and 14 days after the eruption for the noninteractive MA/ECHAM4 simulation.

active simulation is distributed over a larger area, and its maximum is located farther west than that in the noninteractive simulation. Also, a larger amount of the interactively simulated volcanic cloud is found near the equator. Twelve days after the eruption, these differences increase significantly. The volcanic cloud in the interactive simulation is located farther south and west and is much more dispersed than in the noninteractive simulation. Two weeks after the eruption, the cloud has spread from the east Pacific to the west coast of

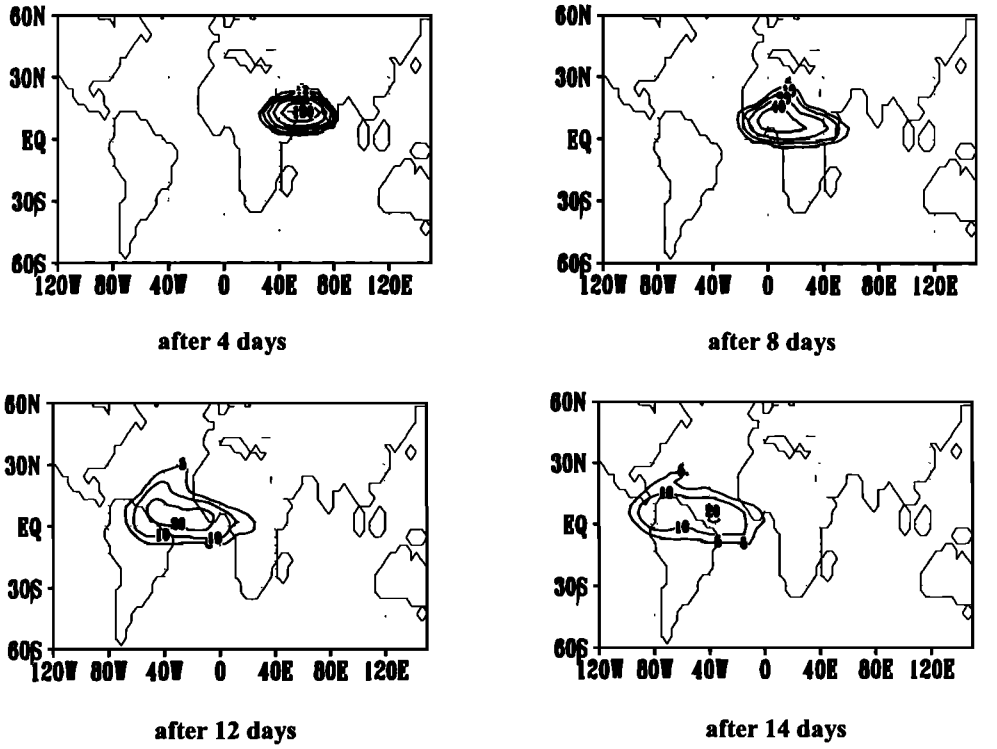

Figure 3. Same as Figure 2, but for the interactive MA/ECHAM4 simulation.

Africa in the interactive simulation, while in the noninteractive simulation the simulated cloud front has only reached the east coast of South America. Overall, the volcanic cloud in the interactive simulation has moved more rapidly westward compared with the noninteractive one. In contrast to the noninteractive simulation, in the interactive case a substantial part of the cloud is found south of the equator. The interactive simulation is therefore capable of simulating the observed initial cross–equatorial transport of the Pinatubo cloud. *Young et al.* [1994] first suggest that the reason for this cross–equatorial transport might be a local perturbation in the temperature and wind fields caused by the additional heating of the volcanic aerosol. Figure 4 shows latitude height cross sections of the zonally averaged SO_2 concentrations in both simulations and the temperature difference between them 12 days after the eruption. Temperature fields of the noninteractive simulation are subtracted from the interactive one, so positive anomalies indicate a warmer interactive simulation. In the interactive case the temperature is about 1–2 K higher in the tropical stratosphere between 10 and 100 hPa. This area coincides with the volcanic aerosol distribution 12 days after the eruption. Temperature perturbations of the order of 1 K also occur in the polar regions and at the top of the atmosphere. The meteorological fields in both model experiments are different, and thus temperature differences between them could be fortuituos and not caused by aerosol–induced heating. However, the strong agreement between aerosol distribution and temperature changes indicates the appearance of aerosol–induced heating due to the enhanced absorption of near–IR ($0.68\ \mu m < \lambda < 4\ \mu m$) and longwave radiation. The additional heating seems to cause a lifting of the volcanic cloud. As the result, in the interactive simulation the bulk of the SO_2 cloud is located at 30 hPa, while in the noninteractive experiment the maximum concentration is found between 40 and 50 hPa. Our results therefore support the findings of *Young et al.* [1994] and *Fairlie* [1995] that absorption of infrared radiation changes the local circulation and leads to an initial cross–equatorial transport. Nevertheless, more calculations under different initial conditions are necessary for a final statement about aerosol–induced heating.

Figure 5 shows simulated vertical profiles of the SO_4^{2-} concentration in the tropical region for the first 6 months after the eruption. Aerosol–induced lifting can be mainly observed in the first 4 months after the eruption. Lifting is therefore an important process in the early stages of our simulation, where the maximum heating rates occur; see Figure 1. Figures 2 and 3 demonstrate how aerosol–induced heating influences the initial dispersal of the volcanic aerosol. One possible way of studying this influence over a longer timescale is the comparison of the geographical distribution of the optical depth in the MA/ECHAM4 simulations and the satellite observations.

3.3. Optical Depth

In Figure 6, the simulated stratospheric optical depth τ at 0.5 μm for both the interactive and the noninteractive experiment is compared with advanced very high resolution radiometer (AVHRR) satellite data at 0.5 μm [*Long and Stowe,* 1994] and Stratospheric Aerosol and Gas Experiment II (SAGE II) data at 0.525 μm [*Thomason et al.,* 1997]. Note that the AVHRR data have overestimated Sun photometer measurements from Mauna Loa and Samoa by about 36% [*Long and Stowe,* 1994]. *Russell et al.* [1996] recommended a factor of 0.84 for the satellite data from June to December 1991 as a result of data comparison.

One of the major differences between the interactive and noninteractive experiments, shown in Figure 6, is the geographical distribution of the tropical aerosol maximum. As a result of the initial cross–equatorial transport, the tropical maximum in the interactive case is shifted equatorward, similar to observations, while in the noninteractive case the aerosol cloud maximum is located at 10°N. Nevertheless, the meridional transport across the equator seems to be underestimated in both model runs in comparison with the satellite data, where the maximum load is located south of the equator between 0° and 10°S. This was due to a specific synoptic situation during June 1991, when a strong high over Tibet helped to carry the cloud southward. In the first half year after the eruption the simulated optical depth is in very good agreement with the satellite data. The satellite data's local maximum in the Southern Hemisphere from November 1991 to March 1992 comes from the August eruption of Cerro Hudson (45.90°S, 79.96°W), which is not considered in our simulations. In August the tropical maximum of the optical depth in the AVHRR data is $\tau = 0.35$ (uncorrected $\tau^* = 0.475$), while in the noninteractive MA/ECHAM4 simulation the maximum is $\tau = 0.38$ and in the interactive simulation $\tau = 0.35$. Owing to stronger dispersion by aerosol lifting, the maximum values in the interactive simulation (Figures 4 and 5) are slightly reduced in comparison with the noninteractive simulation. The SAGE II values in the equatorial region are smaller than those of the simulations and the AVHRR data, which might be caused by reconstruction problems due to initial supersaturation of the instrument [*Russell et al.,* 1996].

As a result of the mean meridional circulation, a second maximum occurs first in Northern Hemisphere winter 1991/1992 in the midlatitudes and then shifted to high latitudes after the breakdown of the polar vortex. Owing to the lower tropopause, aerosol that is transported from lower latitudes is accumulated at higher latitudes [*Trepte et al.,* 1994]. The simulated formation of this second local maximum between 30°N and 60°N, with an optical depth in the range of $0.19 \leq \tau \leq 0.2$ between December 1991 and May 1992, is in excellent agreement with the SAGE data. In the

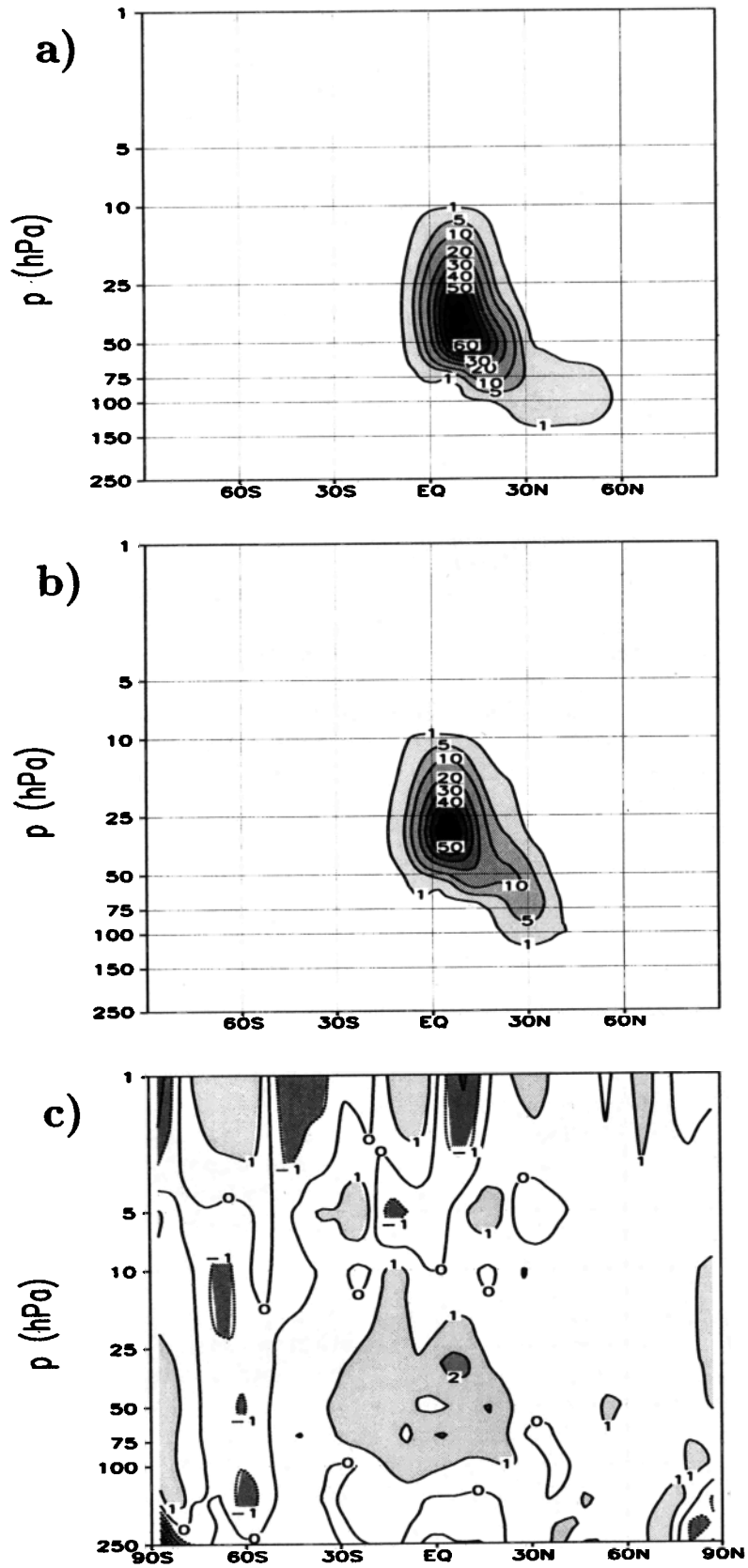

Figure 4. Different model results 12 days after the eruption for SO_2 ($10^{-6}g/m^3$) concentration in the (a) noninteractive and (b) interactive MA/ECHAM4 simulation and (c) temperature difference (K) between the interactive and noninteractive cases. Positive values indicate a warmer interactive simulation.

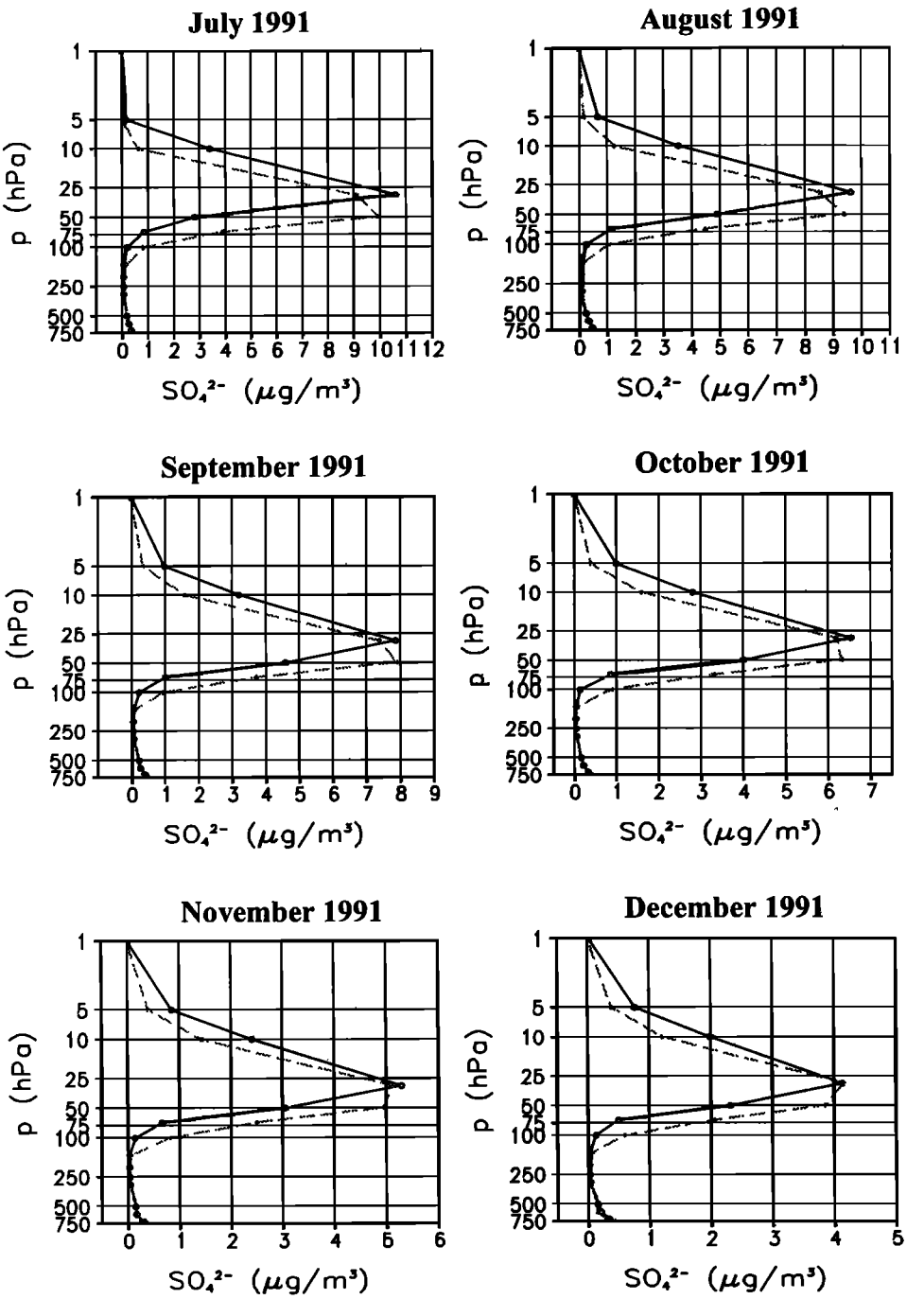

Figure 5. Vertical profiles of the zonal and monthly averaged SO_4^{2-} concentration (10^{-6}g/m^3) at the equator in the first 6 months after the Pinatubo eruption. Solid lines indicate the interactive MA/ECHAM4 simulation, and dashed lines denote the noninteractive one.

AVHRR data the second maximum is postponed by about 3 months, which might be explained by the lack of data poleward of 30°N in autumn 1991. Nevertheless, in situ aircraft measurements and lidar observations showed also that Pinatubo aerosol had already reached high northern latitudes in autumn 1991 [*Beyerle and Neuber*, 1994].

3.4. Tropical Barrier

A notable difference between simulations and observations is the persistence of the tropical maximum. In the satellite data the tropical maximum can be observed until July 1992, while in the simulations a meridional shift to the northern midlatitudes is found. Analyses

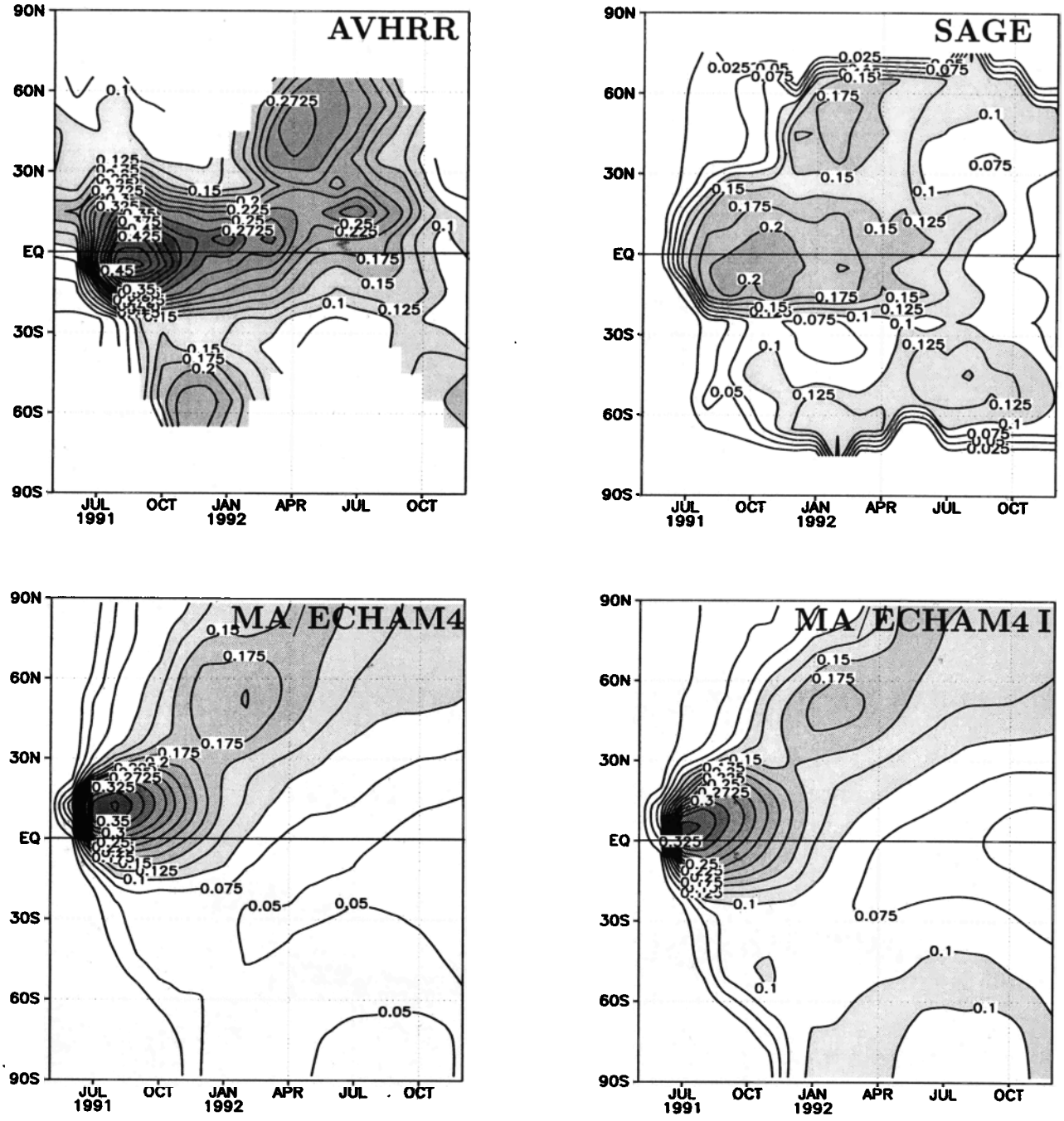

Figure 6. Comparison of the stratospheric optical depth τ for $\lambda = 0.5$ μm between advanced very high resolution radiometer (AVHRR) data [*Long and Stowe*, 1994], Stratospheric Aerosol and Gas Experiment (SAGE) data (τ for λ=0.525 μm) [*Thomason et al.*, 1997] and the MA/ECHAM4 simulation. "I" indicates the interactive case. For the radiative calculations of the ECHAM4 simulation a typical lognormal background distribution with mode radius $r_m = 0.075$ μm and standard deviation $\sigma_s = 1.8$ is assumed.

of SAGE data by *Trepte et al.* [1993] and aircraft measurements by *Jonsson et al.* [1996] showed that in the Northern Hemisphere winter of 1991/1992, two distinct stratospheric transport regimes developed: a lower transport regime below 50 hPa with fast meridional poleward transport and an upper transport regime above 30 hPa, which is characterized by a stratospheric tropical reservoir between 20°S and 20°N. Possible reasons for this tropical aerosol reservoir are subtropical, quasi–permeable barriers with strong potential vorticity (PV) gradients, which inhibit transport of tropical air into the subtropics [*Haynes and McIntyre*, 1987; *Trepte et al.*, 1992]. This tropical reservoir between 21 and 28 km is also strongly influenced by the phase of the QBO

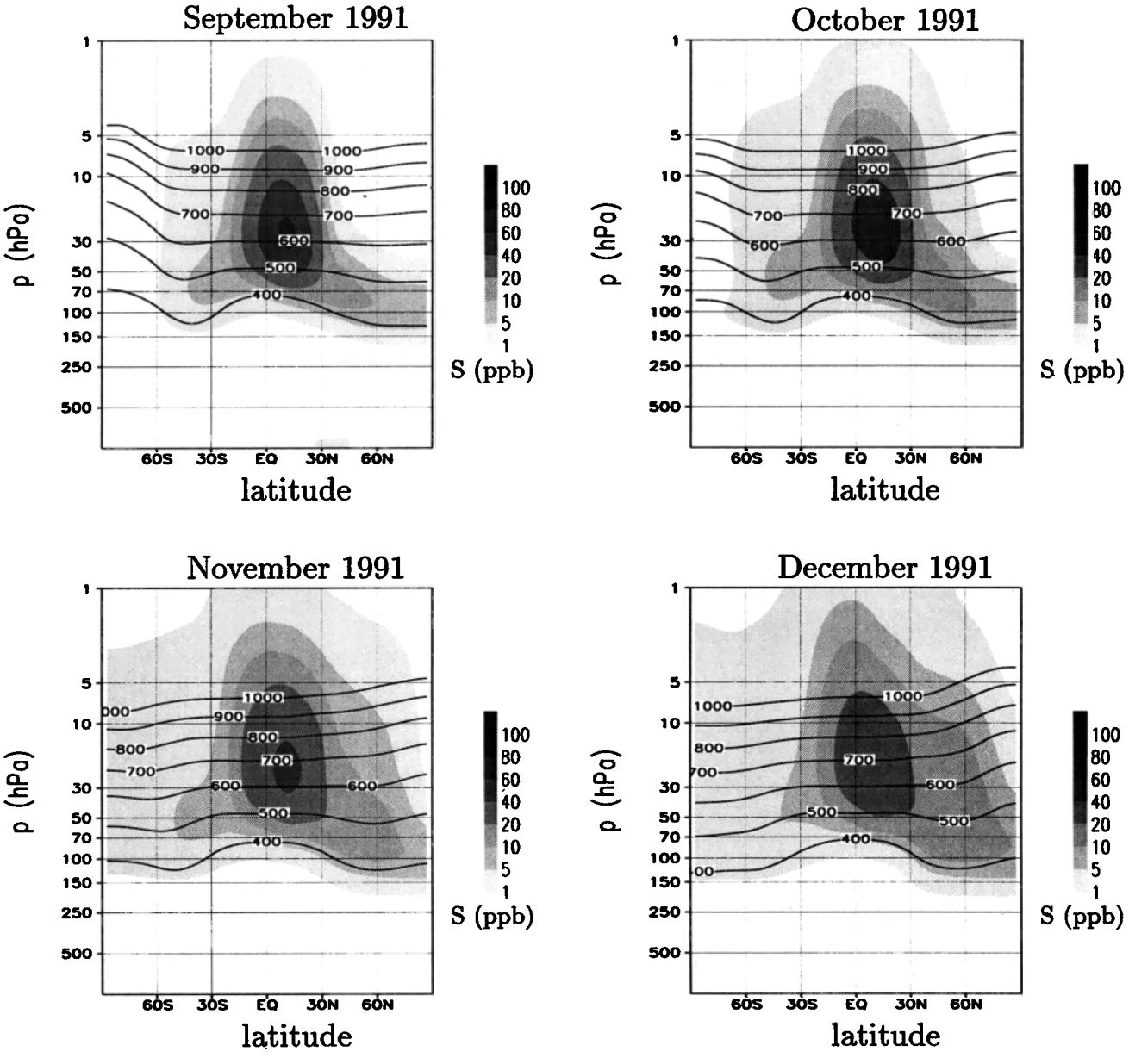

Figure 7. Monthly mean sulfate mass mixing ratios for the noninteractive MA/ECHAM4 simulation. Solid lines indicate isentropic surfaces.

[*Trepte and Hitchman*, 1992]. This reservoir is especially stable during the QBO's easterly shear, where the aerosol tends to remain near the equator, while during the westerly shear the aerosol tends to spread poleward. Mount Pinatubo erupted during the time of a descending QBO's easterly shear, which is thought to be the main reason for the long persistence of the tropical maximum in the observational data.

In our simulation we prescribe only daily observed SSTs. In the MA/ECHAM4, as in all GCMs, the tropical winds are stable easterly, similar to the observed situation in summer 1991. However, the model is not able to properly simulate the QBO. The missing QBO might therefore be one reason that neither the interactive nor the noninteractive simulation is able to simulate the behavior of the tropical aerosol reservoir in 1992. Meridional and vertical transport are strongly connected. If the aerosol sinks downward into the lower transport regime, it may be transported more rapidly to the north. It is thus interesting to see what the vertical distribution of the simulated volcanic cloud looks like in the first months after the eruption.

In Figure 7 and Figure 8, zonal and monthly mean sulfate mass mixing ratios of the noninteractive and the interactive MA/ECHAM4 simulation, respectively, are shown from September 1991 until December 1991. This period encompasses the dispersal of the tropical maximum and the appearance of a second maximum in

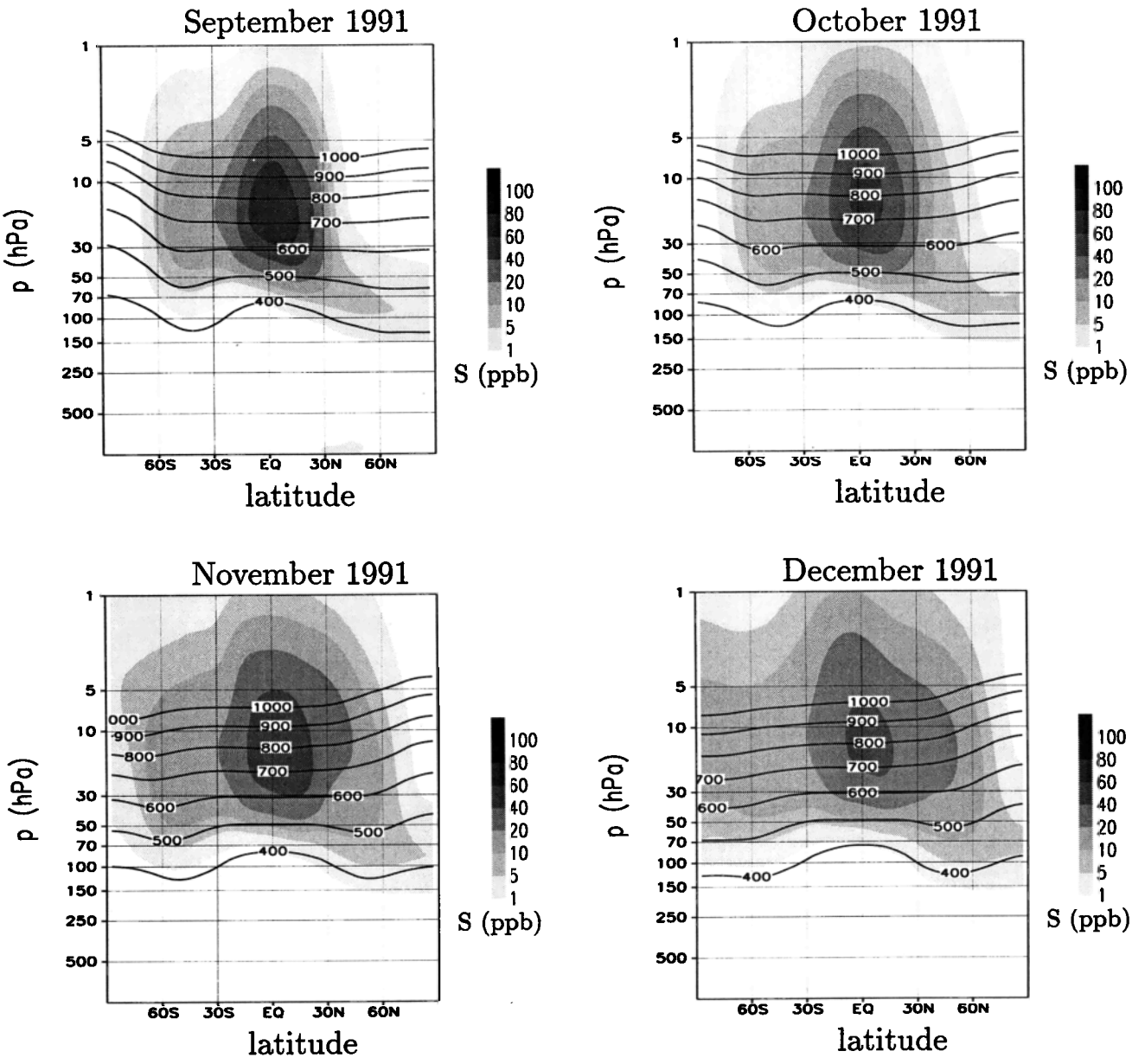

Figure 8. Same as Figure 7, but for the interactive MA/ECHAM4 simulation.

northern midlatitudes. Note that the model results are not density weighted. Owing to the decrease of ambient air density with height, a vertical shift of the sulfur mass mixing ratio results in a decrease of the aerosol concentration.

Aerosol lifting can be clearly observed until October 1991. In September and October the two different transport regimes are well simulated in the Northern Hemisphere in both simulations. Meridional northward transport takes place between 30 and 150 hPa, especially around 70 hPa, and it is mainly connected to synoptic scale disturbances associated with the Asian monsoon [*Trepte et al.*, 1993]. Above 30 hPa the bulk of the aerosol cloud is bound between 30°S and 30°N. Owing to the different vertical and geographical distribution of the volcanic cloud, more aerosol is found in the lower transport regime of the noninteractive simulation. A part of the tropical maximum is located in the interactive simulation south of the equator. The southward transport across the equator is thus enhanced and more realistic mass mixing ratios are found over the Southern Hemisphere.

In October the change from summer to winter circulation takes place, which is associated with an amplification of planetary scale waves in high latitudes. This leads to an enhanced meridional northward transport in November and December in the middle and upper stratosphere. In the noninteractive simulation, the meridional transport decreases with altitude, whereas in the interactive simulation the strongest meridional transport is found between 20 and 5 hPa. Close to 30 hPa, above and below the 600 K isentropic surface,

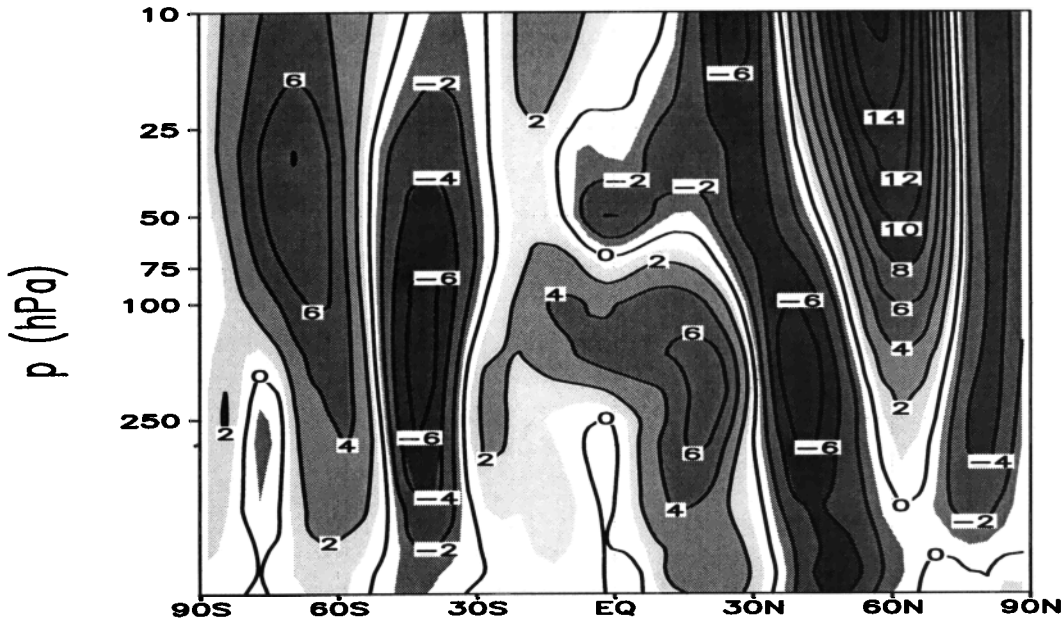

Figure 9. Monthly mean zonal wind differences (m/s) between the interactive and noninteractive MA/ECHAM4 simulations for December 1991.

the meridional transport is reduced in the interactive MA/ECHAM4 simulation and relatively more volcanic material remains in the tropics. This agrees well with tracer studies performed with analyzed UKMO winds for October 1992 to April 1993 by *Chen et al.* [1994], who emphasized that the tropics are most isolated in the middle stratosphere.

In December, volcanic aerosol is found in the polar region between 8 and 150 Pa in the noninteractive experiment whereas the cloud is more affected by the upper stratospheric circulation system in the interactive case. Therefore the poleward transport across the polar circle is much reduced in the Northern Hemisphere, where in winter the developing polar vortex represents an efficient boundary for trace species [e.g., *Tuck,* 1989; *McIntyre,* 1989]. Tracers only enter the polar region in the lowest stratosphere layers in winter. This behavior is consistent with observations made at Spitzbergen and northern Norway during the European Arctic Stratospheric Ozone Experiment (EASOE) campaign in winter 1991/1992 [*Neuber et al.,* 1994].

As indicated in the discussion of Figure 4, temperature and wind changes could not be exclusively related to an aerosol effect. For a definitive statement, ensemble calculation of at least five runs for each experiment have to be performed in order to filter the aerosol effect from the interannual variability. Ensemble simulations with the MA/ECHAM4 model are expensive and thus only useful and successful if the global tracer transport is sufficient. A realistic global aerosol distribution for at least 2 years after the eruption is necessary for the performance of statistical ensembles, which is, at present, not guaranteed with the meridional shift of the tropical maximum at the end of 1991. However, a consideration of wind and temperature changes might be helpful in the interpretation of the different volcanic aerosol distribution in both model runs.

Figure 9 shows a latitude height cross section of the zonal wind differences between the interactive and the noninteractive simulation for December 1991. The differences indicate a weakening of the subtropical jet and an amplification of the polar vortex. This phenomenon begins in October (Figure 10), leading to a strengthened polar night vortex, which is essential for the formation of the observed climate anomalies [*Graf et al.,* 1993]. The strengthened polar vortex is disturbed in midwinter, when the zonal winds relax in the model, as was observed in January 1992. Stratospheric temperature observations in the Northern Hemisphere [*Labitzke,* 1994] show that in January 1992 a minor stratospheric warming occurred. Later, the vortex became stronger again and the minor warming ended. In March and April the same situation, i.e., a stronger than normal polar vortex, was observed. In the model simulation the recovery of the vortex is delayed and it remains strong until May. The simulated temperature differences are consistent with the circulation anomalies, with a colder pole when the polar vortex is enhanced. Figure 11 shows a comparison of simulated temperature differences between both MA/ECHAM4 simulations at 70 hPa with the observed temperature anomalies from the National Center for Environmental Prediction (NCEP) reanalysis data for the first year after the eruption. In general, the model is able to capture the observed anomaly pattern such as a tropical warming with maximum around 30°N and a cooling in high northern latitudes between October and December 1991. The observed positive temperature anomalies at the south pole are

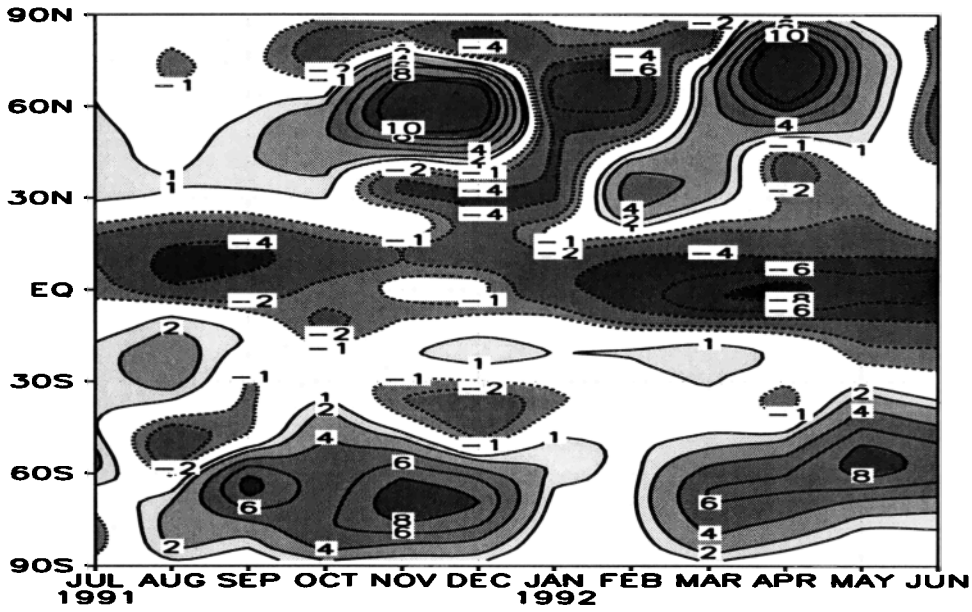

Figure 10. Simulated zonal wind differences (m/s) between the interactive and the noninteractive experiments at 30 hPa.

due to the volcanic eruption of Cerro Hudson. Measurements have demonstrated that Cerro Hudson aerosol had enhanced the stratospheric aerosol concentration south of 55°S in austral spring [*Hofmann et al.*, 1992; *Deshler et al.*, 1992b]. The MA/ECHAM4 simulation is also able to reproduce the warming in January 1992. However, a comparison of absolute values indicates that the simulated absolute temperatures are not as high as the observed ones, although the anomalies were larger than in the observations.

The simulated temperature anomalies are stronger than the observations, by about a factor of 2. The simulated temperature changes represent a direct comparison between the interactive and noninteractive MA/-ECHAM4 simulations, while the temperature anomalies from NCEP reanalysis data are in respect to the 1968–1997 climatology [*Kalnay et al.*, 1996]. In contrast to the observations, the simulated temperature anomalies are therefore strongly influenced by the interannual model variability. A quantitative comparison is therefore useful only if interactive and noninteractive ensemble calculations were performed. Nevertheless, an additional known reason for the overestimated temperature perturbations in the simulation is the neglect of temperature changes associated with the QBO [*Kirchner et al.*, 1998]. During the easterly phase of the QBO, stratospheric cooling can be observed. Thus the effect of Mount Pinatubo in the tropics is about 0.5 K larger than observed [*Angell*, 1997]. In 1991 and 1992, *Grant et al.* [1994] observed an ozone reduction of up to 30% in the region of the densest volcanic cloud and a column decrease of about 20% between 16 and 28 km in the tropics. These aerosol–induced ozone changes also have an important effect on stratospheric temperature and circulation. *Kirchner et al.* [1998] show, with the ECHAM4 climate simulation using the PADS data set, that the positive temperature anomalies produced by the aerosol are reduced owing to the ozone reduction by about 1 K. However, their simulations give only a rough estimate of the effect, because the ozone reduction was prescribed. Thus any feedback mechanisms between aerosol and ozone are neglected, which could also alter the observed response. For future releases we therefore plan simulations with prognostic ozone in order to properly simulate the influence of the Pinatubo–effected ozone changes on the dynamics.

Overall, the interactive treatment of the volcanic aerosol cloud in the simulation leads to a temperature response similar to the observed one. Nevertheless, a realistic representation of the QBO and an interactive treatment of ozone are also important for a realistic representation of the observed transport patterns. This is especially important at the end of 1991.

3.5. Aerosol Mass

The improvement of the interactive treatment of the volcanic plume in comparison with the noninteractive can also be recognized in the temporal development of the global aerosol mass. Figure 12 shows, for both cases, the noninteractive and the interactive ones, a comparison of the simulated global and tropical (between 20°N and 20°S) aerosol mass with high resolution infrared radiation sounder (HIRS) observations [*Baran and Foot*, 1994]. For the tropics the MA/ECHAM simulations show no significant difference in the temporal development of the aerosol mass. The agreement with observations is quite good. For the global aerosol load the effect of an interactive treatment of the aerosol can

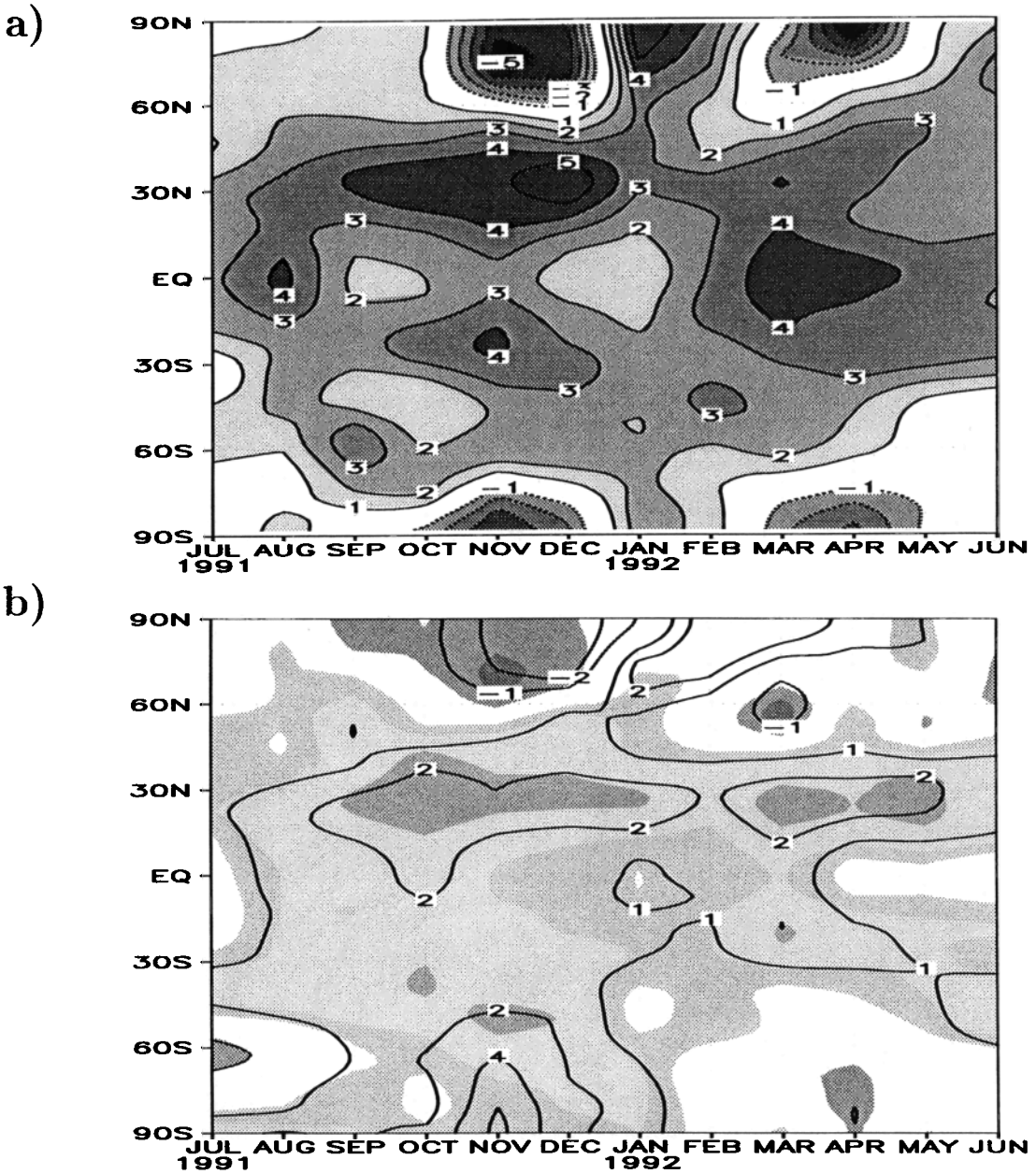

Figure 11. Zonally averaged temperature anomalies at 70 hPa. (a) Temperature difference between the interactive and noninteractive MA/ECHAM4 simulations. (b) Temperature anomalies from National Center for Environmental Prediction reanalysis data with respect to the 1968–1997 climatology [*Kalnay et al.*, 1996]. Shaded areas indicate temperature anomalies larger than 0.5, 1, and 2 standard deviations.

be clearly recognized in the slower decay of the simulated aerosol mass. Six months after the eruption, the differences between both simulations begin to become evident. While the temporal development of the interactive simulation is in good agreement with the satellite data, the aerosol load in the noninteractive simulation declines much more. The stronger decay of the volcanic aerosol in the noninteractive simulation can be explained by the different geographical and vertical distributions of the cloud. Owing to the faster meridional northward transport in the noninteractive simulation, more volcanic aerosol is located in the lower stratosphere and could be transported across the tropopause more rapidly (see also Figures 7 and 8).

3.6. In Situ Measurements

A comparison of model results with in situ measurements confirms the good agreement between simulations and satellite observations in the northern midlatitudes. In Figure 13, monthly mean column mass data of lidar observations at three different stations [*Jäger et al.*, 1995] are compared with simulated val-

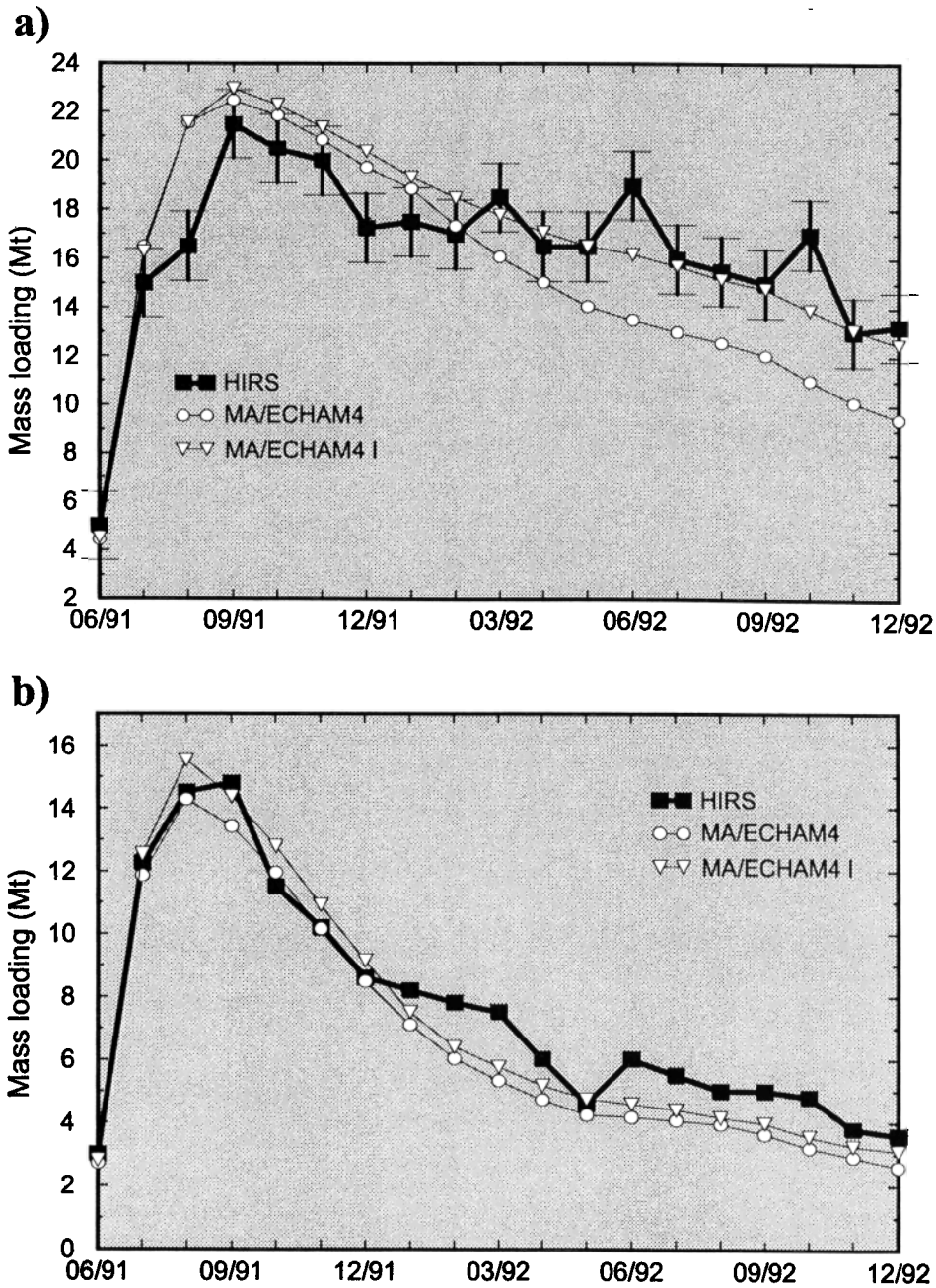

Figure 12. Comparison between ECHAM4 simulations and high-resolution infrared radiometer sounder (HIRS) satellite data [*Baran and Foot,* 1994] of (a) global and (b) tropical sulfate mass loading after the eruption of Mount Pinatubo. The error bars in Figure 12a indicate the uncertainties of the satellite measurements.

ues for the corresponding grid. In the observations the column mass is integrated from above the individually determined tropopause, whereas in the MA/ECHAM4 simulations the column mass represents the sum over the first 27 model layers (250–0.01 hPa). In the first months an improvement due to the interactive treatment of the Pinatubo cloud can be clearly traced. This improvement is especially evident at the midlatitude stations, where the column mass data are determined by meridional northward transport of the cloud from the tropics. Thus, at Garmisch and Tsukuba, a strong increase in the column mass can be observed since October 1991. Owing to the strong meridional northward transport, the noninteractive experiment overestimates the increase of the column mass, while the interactive simulation is in better agreement with the observations.

In contrast to the northern midlatitude stations, Naha is located in the latitude band between 20°S and 30°N, in which the bulk of the aerosol mass was banded in the first months after the eruption [*McCormick and Veiga,*

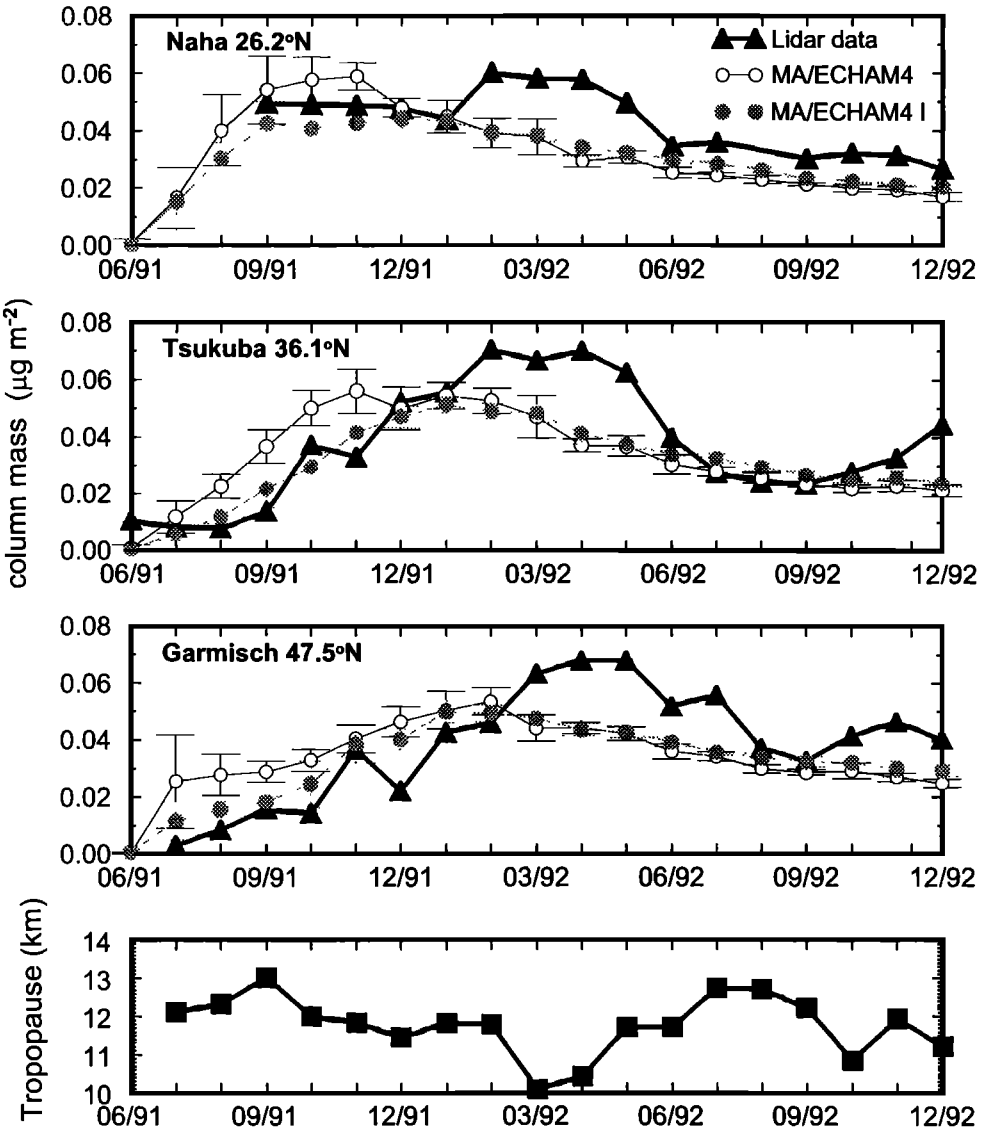

Figure 13. Comparison of observed monthly mean colum mass data [*Jäger et al.,* 1995] at three different stations, Naha, Tsukuba and Garmisch, and simulated values for the corresponding grid, and (bottom) tropopause height at Garmisch. Error bars indicate the standard deviation of the simulated values.

1992; *Stowe et al.,* 1992]. Hence, in the subtropics, the simulated and observed column mass is nearly constant, with a slight decrease over the first months. In January 1991, 7 months after the eruption, the column mass decreases in both simulations in contrast to the observations, but after 12 months (14 months at Garmisch), simulations and observations are in the same range again. The lidar observations in the northern midlatitudes are strongly influenced by seasonal variations of the tropopause height and by STE processes. In winter and spring, with a relatively low tropopause, more aerosol, possibly of tropospheric origin, can be detected in the lower stratosphere by the lidar than in summer and autumn with a relatively high tropopause (Figure 13). Owing to the coarse resolution (both horizontal and vertical) of the atmospheric model, the simulations cannot predict these changes in the column mass, which are influenced by the seasonal variations of the tropopause height. Thus, in contrast to the lidar data, a decrease of the aerosol column mass is simulated in both model simulations throughout 1992. However, during the first 7 months after the eruption and again in the boreal summer of 1992, the interactive MA/ECHAM4 simulation is in good agreement with the lidar data.

Figure 14 shows a comparison of simulated aerosol mass concentrations with measurements from Laramie, Wyoming (41.2 °N) [*Deshler et al.,* 1992a, 1993] for three different heights. Note that in Figure 14, balloon–borne measurements for specific days are compared with monthly mean GCM results for the corresponding grid cell. Thus the measured aerosol concentration reflects synoptic scale transport processes, such as the distinct

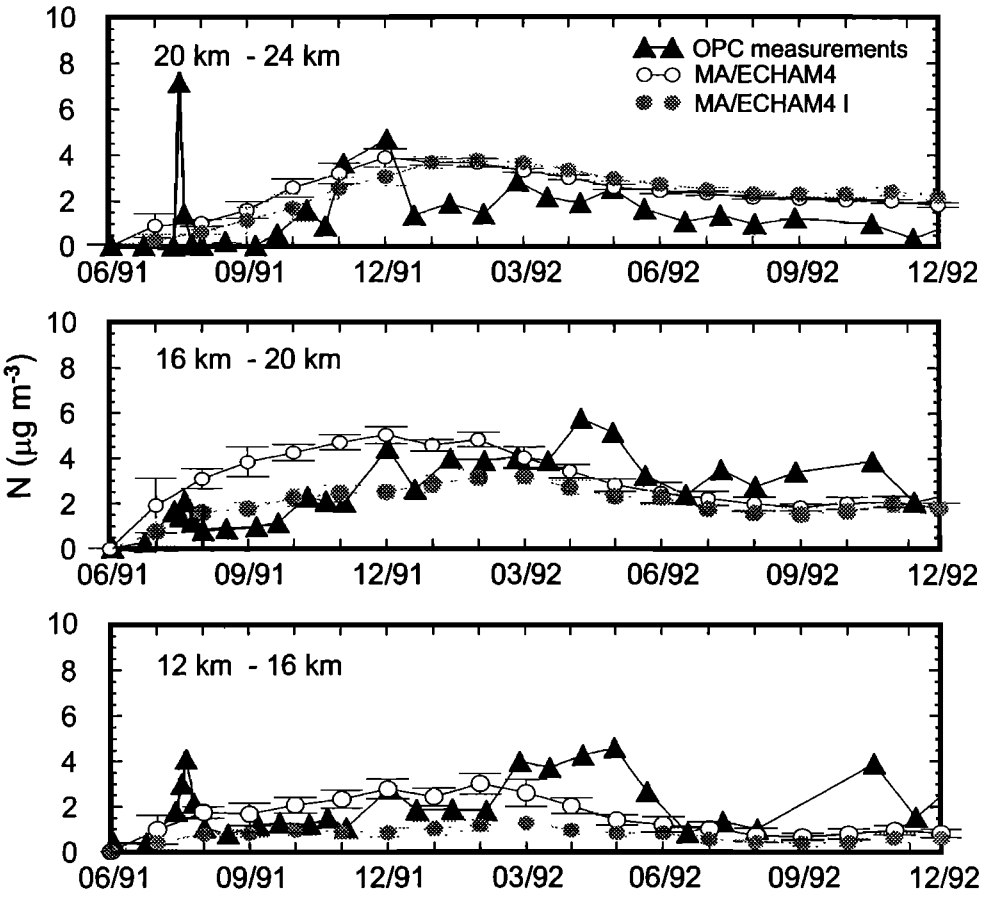

Figure 14. Comparison of individual observed aerosol mass concentrations [*Deshler et al.*, 1993] at three different heights with simulated monthly mean values for the corresponding grid. Error bars indicate the standard deviation of the simulated values.

maximum in July 1991, which are not considered in the model simulations. Assimilated model runs would be better suitable for a comparison of day values.

Generally, the observed aerosol concentrations at Laramie are well represented by the MA/ECHAM4 simulations. In the first half year after the eruption, the interactive simulation is in much better agreement with the balloon data than the noninteractive one. This difference is especially evident in the layer between 16 and 20 km, where the zonal mean aerosol concentration in the noninteractive simulation is twice as high as the interactive simulation and the observations. This is probably due to the enhanced northward and downward transport in the noninteractive model simulation (Figure 7). One year after the eruption, no significant differences between the different MA/ECHAM4 simulations can be detected. In the layer between 20 and 24 km both model simulations overestimate the aerosol concentration by a factor of 2. A possible explanation for this might be the disappearance of the tropical maximum in the model, combined with an increased meridional transport (see also Figures 6-8). The aerosol concentration in the 12-16 km layer, like the column mass, is strongly influenced by the seasonal variations of the tropopause (see also Figure 13). The MA/ECHAM4 simulations could therefore not match the observed increase in the aerosol concentration in Northern Hemisphere spring, which reflects the relative low tropopause.

Overall, the interactive treatment of volcanic aerosol provides an improvement over the model results. Although only prescribed SSTs are used, the interactive MA/ECHAM4 simulation agrees well, most of the time, with Northern Hemisphere station data. Further agreement would probably be reached if the simulations are run in an assimilated mode.

3.7. Flux anomalies

Figure 15 shows, for both the all- and clear-sky cases, changes of the zonal mean net radiative flux at the top of the atmosphere, the tropopause, and the surface. The net radiative flux is strongly influenced by underlying clouds. Differences between all- and clear-sky are largest in the tropical region, especially in the ITCZ, where the highest cloud density is found. In general, the all-sky net fluxes are reduced by one third of the clear-sky fluxes. All-sky and clear-sky net fluxes also differ in their vertical structure. In the clear-

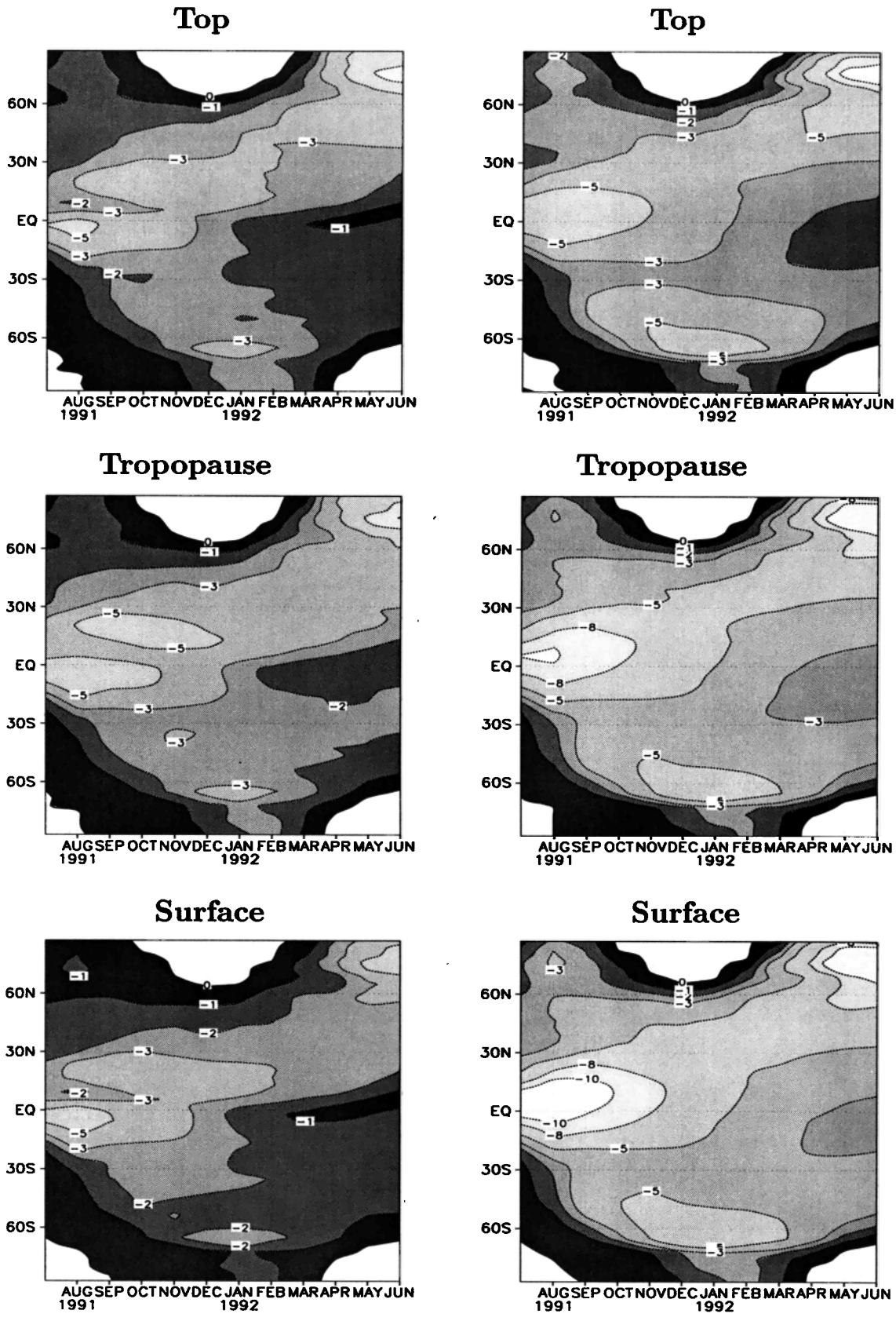

Figure 15. Zonally averaged (left) all–sky and (right) clear–sky net radiative fluxes (W/m^2) at the (top) top of the atmosphere, (middle) tropopause and (bottom) surface.

sky case the net cooling decreases from the surface to the TOA. Although the largest negative net clear–sky fluxes, which are due to scattering processes, occur in the solar part of the aerosol–containing layers, they are partially compensated by the positive net fluxes caused by the thermal irradiation of the aerosol. Because of multiple scattering between the stratospheric aerosol and the tropospheric clouds, the largest negative net fluxes occur in the all–sky case at the tropopause. Thus the relatively strong influence of tropospheric cloudiness on the net radiative forcing emphasizes the importance of on–line calculated radiative forcing rates. A comparison of our net radiative fluxes with the one calculated by *Stenchikov et al.* [1998] shows that our all–sky net radiative fluxes agree well with their values. They also obtain the largest negative net flux of -5 W/m^2 at the tropopause. In contrast to the all–sky simulation, the clear–sky simulation is different from the findings by *Stenchikov et al.* [1998], who estimate the largest net cooling in the tropopause region. A possible reason for these differences might be the different vertical resolution of both models and the different radiative properties of the aerosol.

Minnis et al. [1993] analyzed Earth Radiation Budget Experiment (ERBE) data [*Barkstrom,* 1984] between 40°N and 40°S from May through October 1991. The ERBE data indicate a reduction of 8 W/m^2 of the TOA forcing between 5°S and 5°N and of 4.3 W/m^2 between 40°S and 40°N for August 1991. These data referred to a 5 year average with annual variations in the range of ±3 W/m^2 over the detection area. In the interactive MA/ECHAM4 simulation we get a net radiative cooling of -4.9 W/m^2 between 5°S and 5°N and -2.8 W/m^2 between 40°S and 40°N. Thus the simulated forcing is only two thirds of the observed one. The simplified radiative calculation with a prescribed fixed aerosol size distribution might be one reason for the reduced cooling in the simulations. Another possible reason for this difference might be the sensitivity of radiative forcing to its definition [*Stenchikov et al.,* 1998]. In our simulation we determine the forcing with radiative calculations with and without volcanic aerosol. Thus we neglect any stratospheric temperature perturbation in our radiative calculation and may therefore underestimate the forcing by about 1 to 2 W/m^2 [*Stenchikov et al.,* 1998].

Overall, the net radiative flux is strongly determined by the geographical distribution of the volcanic aerosol. Owing to the short persistence of the tropical aerosol maximum, the calculated net radiative fluxes in the tropics are unrealistic in 1992. Hence climate simulations with prognostical aerosol are currently limited by the three–dimensional transport.

4. Summary and Conclusions

We have performed noninteractive and interactive Pinatubo simulations with the MA/ECHAM4 model. These experiments show that an interactive coupling of the aerosol with the radiation scheme is necessary to adequately adequately describe the observed transport characteristics over the first months after the eruption. The interactive MA/ECHAM4 simulation is able to simulate the initial southward cross–equatorial transport of the cloud as well as aerosol lifting to higher altitudes. An additional improvement of the interactive simulation is a reduced northward transport and an enhanced meridional transport toward the south, which is consistent with observations. The model results agree well with satellite observations and in situ measurements from northern midlatitudes. The MA/ECHAM4 simulations are able to represent the formation of two distinct maxima in the optical depth, but they fail to reproduce the tropical aerosol reservoir since December 1991. One reason for the fast decay of the tropical maximum seems to be the missing QBO in the simulations, which has an important influence on the tropical reservoir. For further studies we therefore plan an interactive MA/ECHAM4 Pinatubo simulation with assimilated QBO wind fields. A performance of the simulation with a better horizontal resolution might also be useful to improve the duration of the tropical maximum.

The simulated dynamic feedback in the interactive model simulation is similar to observations. The model is able to simulate the strengthening of the polar night vortex in winter 1991/1992 and a warming in midwinter. The dynamic response in the model seems to be overestimated, possibly owing to the neglect of ozone changes.

However, ensemble calculations are necessary to estimate the climate response of the Pinatubo eruption with the MA/ECHAM4 model and to relate dynamic perturbations to the volcanic aerosol. For the successful performance of ensemble simulations with the MA/ECHAM4 certain aspects have to be guaranteed as follows:

1. The three-dimensional tracer transport must be sufficient. A realistic global aerosol distribution for at least 2 years after the eruption is necessary, with a better representation of the tropical maximum.

2. Ozone changes should be regarded in the model. The observed ozone depletion leads to less absorption of solar heating in low latitudes and thus to a damping of the temperature feedback. In order to properly simulate the observed ozone changes, an interactive chemical and microphysical module is necessary, which is currently in development.

3. For a realistic determination of the radiative forcing of the Pinatubo aerosol, microphysical processes of the formation and the development of stratospheric aerosol must be considered.

4. The influence on the QBO of the stratospheric tracer transport has be taken into account.

Generally, the interactive treatment of the volcanic aerosol represents a considerable improvement for the global transport of the cloud, but there are still some critical points that must be solved in the future.

Acknowledgments. The authors would like to thank Johann Feichter for helpful discussions. Furthermore, we are grateful to Terry Deshler, Horst Jäger, Larry Stowe, and Larry Thomason for providing their data and Christoph Brühl for the chemical input data. This work was supported by the Bundesministerium für Bildung, Wissenschaft, Forschung und Technologie (BMBF) grant 01 L0 9512/0 (project OFP).

References

Angell, J. K., Stratospheric warming due to Agung, El Chichón, and Pinatubo taking into account the quasi-biennial oscillation, *J. Geophys. Res., 102,* 9479–9485, 1997.

Baran, A. J., and J. S. Foot, New application of the operational sounder HIRS in determining a climatology of sulphuric acid aerosol from the Pinatubo eruption, *J. Geophys. Res., 99,* 25,673–25,679, 1994.

Barkstrom, B. R., The Earth Radiation Budget Experiment (ERBE), *Bull. Am. Meteorol. Soc., 65,* 1170–1185, 1984.

Bekki, S., and J. A. Pyle, A two-dimensional modeling study of the volcanic eruption of Mount Pinatubo, *J. Geophys. Res., 99,* 18,861–18,869, 1994.

Beyerle, G., and R. Neuber, The stratospheric aerosol content above Spitsbergen during winter 1991/92, *Geophys. Res. Lett., 21,* 1291–1294, 1994.

Bluth, G. J. S., S. D. Doiron, C. C. Schnetzler, A. J. Krueger, and L. S. Walter, Global tracking of the SO_2 clouds from the June 1991 Mount Pinatubo eruptions, *Geophys. Res. Lett., 19,* 151–154, 1992.

Boville, B. A., J. R. Holton, and P. W. Mote, Simulation of the Pinatubo aerosol cloud in general circulation model, *Geophys. Res. Lett., 18,* 2281–2284, 1991.

Brasseur, G., and C. Granier, Mount Pinatubo aerosols, chloroflurocarbons and ozone depletion, *Science, 257,* 1239–1242, 1992.

Chen, P., J. R. Holton, A. O Neill and R. Swinbank, Isentropic mass exchange between the tropics and the extratropics in the stratosphere, *J. Atmos. Sci., 51,* 3006–3018, 1994.

Coffey, M. T., Observations of the impact of volcanic activity on stratospheric chemistry, *Geophys. Res. Lett., 101,* 6767–6780, 1996.

Coffey, M. T., and W. G. Mankin, Observations of the loss of stratospheric NO_2 following volcanic eruptions, *Geophys. Res. Lett., 20,* 2873–2876, 1993.

Deshler, T., D. J. Hofmann, B. J. Johnson, and W. R. Rozier, Balloonborne measurements of the Pinatubo aerosol size distribution and volatility at Laramie, Wyoming during the summer of 1991, *Geophys. Res. Lett., 19,* 199–203, 1992a.

Deshler, T., A. Adriani, G. P. Gobbi, D. J. Hofmann, G. Di Donfranceso, and B. J. Johnson, Volcanic aerosol and ozone depletion within the Antarctic polar vortex during the austral spring of 1991, *Geophys. Res. Lett., 19,* 1819–1822, 1992b.

Deshler, T., B. J. Johnson, and W. R. Rozier, Balloonborne measurements of Pinatubo aerosol during 1991 and 1992 at 41° N: Vertical profiles, size distribution, and volatility, *Geophys. Res. Lett., 20,* 1435–1438, 1993.

Dutton, E. G., and J. R. Christy, Solar radiative forcing at selected locations and evidence for global lower tropospheric cooling following the eruptions of El Chichón and Pinatubo, *Geophys. Res. Lett., 19,* 2313–2316, 1992.

Fairlie, T. D. A., Three-dimensional transport simulations of the dispersal of volcanic aerosol from Mount Pinatubo, *Q. J. R. Meteorol. Soc., 121,* 1943–1980, 1995.

Feichter, J., E. Kjellström, H. Rodhe, F. Dentener, J. Lelieveld, and G.-J. Roelofs, Simulation of the tropospheric sulfur cycle in a global climate model, *Atmos. Environ., 30,* 1693–1707, 1996.

Fouquart, Y., and B. Bonnel, Computations of solar heating of the earth atmosphere: A new parameterization, *Contrib. Atmos. Phys., 53,* 35–62, 1980.

Graf, H.-F., I. Kirchner, A. Robock, and I. Schult, Pinatubo eruption winter climate effects: Model versus observation, *Clim. Dyn., 9,* 81–93, 1993.

Graf, H.-F., I. Kirchner, and I. Schult, Modelling Mt. Pinatubo climate effects, in *The Mount Pinatubo Eruption Effects on the Atmosphere and Climate, NATO ASI Ser., Ser. I,* vol. 42, edited by G. Fiocco, D. Fua, and G. Visconti, pp. 219–232, Springer–Verlag, New York, 1996.

Grant, W. B., et al., Aerosol–associated changes in tropical stratospheric ozone following the eruption of Mount Pinatubo, *J. Geophys. Res., 99,* 8197–8211, 1994.

Grant, W. B., et al., Observations of reduced ozone concentrations in the tropical stratosphere after the eruption of Mt. Pinatubo, *Geophys. Res. Lett., 19,* 1109–1112, 1992.

Grooß, J. U., C. Brühl, and T. Peter, Impact of aircraft emissions on tropospheric and stratospheric ozone. Part I: Chemistry and 2-D model results, *Atmos. Environ., 32,* 3173–3184, 1998.

Hansen, J., R. Ruedy, and M. Sato, Potential climate impact of Mount Pinatubo, *Geophys. Res. Lett., 19,* 215–218, 1992.

Hansen, J., et al., in *The Mount Pinatubo Eruption Effects on the Atmosphere and Climate, NATO ASI Ser., Ser. I,* vol. 42, edited by G. Fiocco, D. Fua, and G. Visconti, pp. 233–272, Springer–Verlag, New York, 1996.

Haynes, P. E., and M. E. McIntyre, On the evolution of vorticity and potential vorticity in the presence of diabatic heating, *J. Atmos. Sci., 44,* 828–841, 1987.

Herman, J. R., and D. Larko, Low ozone amounts during 1992–1993, *J. Geophys. Res., 99,* 3483–3496, 1994.

Hofmann, D. J., and S. Solomon, Ozone destruction through heterogeneous chemistry following the eruption of El Chichón, *J. Geophys. Res., 94,* 5029–5041, 1989.

Hofmann, D. J., S. J. Oltmans, J. M. Harris, S. Solomon, T. Deshler, and B. J. Johnson, Observation and possible causes of new ozone depletion in Antarctica in 1991, *Nature, 359,* 283–287, 1992.

Hofmann, D. J., and S. J. Oltmans, Anomalous antarctic ozone during 1992: Evidence for Pinatubo volcanic aerosol effects, *J. Geophys. Res., 98,* 18,555–18,561, 1993.

Jäger, H., The Pinatubo eruption cloud observed by lidar at Garmisch–Partenkirchen, *Geophys. Res. Lett., 19,* 191–194, 1992.

Jäger, H., O. Uchino, T. Nagai, T. Fujimoto, V. Freudenthaler, and F. Homburg, Ground–based remote sensing of the decay of the Pinatubo eruption cloud at three northern hemisphere sites, *Geophys. Res. Lett., 22,* 607–610, 1995.

Johnston, P. V., R. L. McKenzie, J. G. Keys, and W. A. Matthews, Observation of depleted stratospheric NO_2 following the Pinatubo volcanic eruption, *Geophys. Res. Lett., 19,* 211–213, 1992.

Jonsson, H. H., J. C. Wilson, C. A. Brock, J. E. Dye, G. V. Ferry, and K. R. Chan, Evolution of the stratospheric aerosol in the northern hemisphere following the June 1991 volcanic eruption of Mount Pinatubo: Role of tropospheric–stratospheric exchange and transport, *J. Geophys. Res., 102,* 1553–1570, 1996.

Kalnay, E., et al., The NCEP/NCAR 40–year reanalysis project, *Bull. Am. Meteorol. Soc., 77,* 437–471, 1996.

Kinne, S., O. B. Toon, and M. J. Prather, Buffering of stratospheric circulation by changing amounts of tropi-

cal ozone: A Pinatubo case study, *Geophys. Res. Lett., 19,* 1927–1930, 1992.

Kinnison, D. E., K. E. Grant, P. S. Connell, D. A. Rotman, and D. J. Wuebbles, The chemical and radiative effects of the Mount Pinatubo eruption, *J. Geophys. Res., 99,* 25,705–25,731, 1994.

Kirchner, I., G. L. Stenchikov, H.-F. Graf, A. Robock and J. C. Antuña, Climate model simulation of winter warming and summer cooling following the 1991 Mount Pinatubo eruption, *Rep. 261,* 35 pp., Max–Planck–Inst. für Meteorol., Hamburg, Germany, 1998.

Kodera, K., Infuence of volcanic eruptions on the troposphere through stratospheric dynamical processes in the Northern Hemisphere winter, *J. Geophys. Res., 99,* 1273–1282, 1994.

Koike, M., N. B. Jones, W. A. Matthews, P. V. Johnston, R. L. McKenzie, D. Kinnison, and J. Rodriguez, Impact of Pinatubo aerosols on the partitioning between NO_2 and HNO_3, *J. Geophys. Res., 21,* 597–600, 1994.

Krueger, A. J., L. S.Walter, P. K. Bhartia, C. C. Schnetzler, N. A. Krotkov, I. Sprod, and G. J. S. Bluth, Volcanic sulfur dioxide measurements from the total ozone mapping spectrometer instruments, *J. Geophys. Res., 100,* 14,057–14,076, 1995.

Labitzke, K., Stratospheric temperature changes after the Pinatubo eruption, *J. Atmos. Terr. Phys., 56,* 1027–1034, 1994.

Labitzke, K., and M. P. McCormick, Stratospheric temperature increases due to Pinatubo aerosols, *Geophys. Res. Lett., 19,* 207–210, 1992.

Long, C. S., and L. L. Stowe, Using the NOAA/AVHRR to study stratospheric aerosol optical thickness following the Mt. Pinatubo eruption, *Geophys. Res. Lett., 21,* 2215–2218, 1994.

Manzini, E., N. A. McFarlane, and C. McLandress, Impact of the Doppler spread parameterization on the simulation of the middle atmosphere circulation using the MA/ECHAM4 general circulation model, *J. Geophys. Res., 102,* 25,751–25,762, 1997.

McCormick, M. P. and R. E. Veiga, SAGE II measurements of early Pinatubo aerosols, *Geophys. Res. Lett., 19,* 155–158, 1992.

McCormick, M. P., L. W. Thomason, and C. R. Trepte, Atmospheric effects of the Mt. Pinatubo eruption, *Nature, 373,* 399–404, 1995.

McIntyre, M. E., On the Antarctic ozone hole, *J. Atmos. Terr. Phys., 51,* 29–34, 1989.

Minnis, P., E. F. Harrison, L. L. Stowe, G. G. Gibson, F. M. Denn, D. R. Doelling, and W. L. Smith Jr., Radiative climate forcing by the Mount Pinatubo eruption, *Science, 259,* 1411–1415, 1993.

Morcrette, J. J., Radiation and cloud radiative properties in the ECMWF operational weather forecast model, *J. Geophys. Res., 96,* 9121–9132, 1991.

Neuber, R., et al., Latitudinal distribution of stratospheric aerosols during the EASOE winter 1991/92, *Geophys. Res. Lett., 21,* 1283–1286, 1994

Pinnick, R. G, J. M. Rosen, and D. J. Hofmann, Stratospheric aerosol measurements, III: Optical model calculations, *J. Atmos. Sci., 33,* 304–314, 1976.

Pitari, G., A numerical study of the possible perturbation of stratospheric dynamics due to Pinatubo aerosols: Implications for tracer transport, *J. Atmos. Sci., 50,* 2443–2461, 1993.

Prather, M., Catastrophic loss of stratospheric ozone in dense volcanic clouds, *J. Geophys. Res., 97,* 10,187–10,191, 1992.

Pudykiewicz, J. A., and A. P. Dastoor, On numerical simulation of the global distribution of sulfate aerosol produced by a large volcanic eruption, *J. Clim., 8,* 464–473, 1995.

Randel, W. J., F. Wu, J. M. Russell III, J. W. Waters, and L. Froidevaux, Ozone and temperature changes in the stratosphere following the eruption of Mount Pinatubo, *J. Geophys. Res., 100,* 16,753–16,764, 1995.

Read, W.G., L. Froidevaux, and J. W. Waters, Microwave limb sounder measurements of stratospheric SO_2 from the Mt. Pinatubo volcano, *Geophys. Res. Lett., 20,* 1299–1302, 1993.

Robock, A., and J. Mao, Winter warming from large volcanic eruptions, *Geophys. Res. Lett., 19,* 2405–2408, 1992.

Robock, A., and J. Mao, The volcanic signal in surface temperature observations, *J. Clim., 8,* 1086–1103, 1995.

Roeckner, E., K. Arpe, L. Bengtsson, M. Christoph, M. Claussen, L. Dümenil, M. Esch, M. Giorgetta, U. Schlese, and U. Schulzweida, The atmospheric general circulation model ECHAM-4: Model description and simulation of the present-day climate, *Rep. 218,* Max–Planck–Inst. für Meteorol., Hamburg, Germany, 1996.

Roelofs, G. J., and J. Lelieveld, Distribution and budget of O_3 in the troposphere calculated with a chemistry general circulation model, *J. Geophys. Res., 100,* 20,983–20,998, 1995.

Russell, P. B., et al., Global to microscale evolution of the Pinatubo volcanic aerosol, derived from diverse measurements and analyses, *J. Geophys. Res., 101,* 18,745–18,763, 1996.

Schoeberl, M. R., P. K. Bhartia, and E. Hilsenrath, Tropical ozone loss following the eruption of Mt. Pinatubo, *J. Geophys. Res., 20,* 29–32, 1993.

Solomon, S., R. W. Portmann, R. R. Garcia, L. W. Thomason, L. R. Poole, and M. P. McCormick, The role of aerosol variations in anthropogenic ozone depletion at northern midlatitudes, *J. Geophys. Res., 101,* 6713–6727, 1996.

Steil, B., M. Dameris, C. Brühl, P. J. Crutzen, V. Grewe, M. Ponater, and R. Sausen, Development of a chemistry module for GCMs: First results of a multi-annual integration, *Ann. Geophys., 16,* 205–228, 1998.

Stenchikov, G. L., I. Kirchner, A. Robock, H.-F. Graf, J. C. Antuna, R. Grainger, A. Lambert, and L. Thomason, Radiative forcing from the 1991 Mt. Pinatubo volcanic eruption, *J. Geophys. Res., 103,* 13,837–13,858, 1998.

Stowe, L. L., R. M. Carey, and P. P. Pellegrino, Monitoring the Mt. Pinatubo aerosol layer with NOAA/11 AVHRR data, *Geophys. Res. Lett., 19,* 159–162, 1992.

Thomason, L. W., L. R. Poole, and T. Deshler, A global climatology of stratospheric aerosol surface area density deduced from Stratospheric Aerosol and Gas Experiment II: 1984-1994, *J. Geophys. Res., 102,* 8967–8976, 1997.

Tie, X., G. P. Brasseur, B. Briegleb, and C. Granier, Two-dimensional simulation of Pinatubo aerosol and its effect on stratospheric ozone, *J. Geophys. Res., 99,* 20,545–20,562, 1994.

Timmreck, C., H.-F. Graf and J. Feichter, Simulation of Mt. Pinatubo aerosol with the Hamburg climate model ECHAM4, *Theor. Appl. Climatol.,* in press, 1999.

Trepte, C. R., and M. H. Hitchman, Tropical stratospheric circulation deduced from satellite aerosol data, *Nature, 355,* 626–628, 1992.

Trepte, C. R., R. V. Veiga, and M. P. McCormick, The poleward dispersal of Mount Pinatubo volcanic aerosol, *J. Geophys. Res., 98,* 18,563–18,573, 1993.

Trepte, C. R., L. W. Thomason and G. S. Kent, Banded structures in stratospheric aerosol distributions, *Geophys. Res. Lett., 21,* 2397–2400, 1994.

Tuck, A. F., Synoptic and chemical evolution of the Antarctic vortex in late winter and early spring 1987, *J. Geophys. Res., 94,* 11,687–11,737, 1989.

Weisenstein, D. K., G. K. Yue, M. K. W. Ko, N.-D. Sze, J. M. Rodriguez, and C. J. Scott, A two–dimensional model of sulfur species and aerosols, *J. Geophys. Res., 102,* 13,019–13,053, 1997.

Williamson, D. L., and P. J. Rasch, Two–dimensional semi–lagrangian transport with shape–preserving interpolation, *Mon. Weather Rev., 117,* 102–129, 1989.

Young, R. E., H. Houben, and O. B. Toon, Radiatively forced dispersion of the Mt. Pinatubo volcanic cloud and induced temperature perturbations in the stratosphere during the first few months following the eruption, *Geophys. Res. Lett., 21,* 369–372, 1994.

Zhao, J., R. P. Turco, and O. B. Toon, A model simulation of Pinatubo volcanic aerosols in the stratosphere, *J. Geophys. Res., 100,* 7315–7328, 1995.

H-F. Graf, I. Kirchner, and C. Timmreck, Max–Planck Institut für Meterologie, Bundesstrasse 55, D-20146 Hamburg, Germany (e-mail: timmreck@dkrz.de)

(Received July 13, 1998; revised November 24, 1998; accepted February 4, 1999.)